Motion between the Indian, Capricorn and Somalian plates since 20 Ma: implications for the timing and magnitude of distributed lithospheric deformation in the equatorial Indian ocean

Charles DeMets,[1] Richard G. Gordon[2] and Jean-Yves Royer[3]

[1]*Department of Geology and Geophysics, University of Wisconsin-Madison, Madison, WI 53706 USA. E-mail: chuck@geology.wisc.edu*
[2]*Department of Earth Science, Rice University, Houston, TX 77005 USA. E-mail: rgg@rice.edu*
[3]*CNRS, UBO-IUEM Domaines Océaniques, 29280 Plouzané, France. E-mail: jyroyer@univ-brest.fr*

SUMMARY

Approximately 2200 magnetic anomaly crossings and 800 fracture zone crossings flanking the Carlsberg ridge and Central Indian ridge are used to estimate the rotations of the Indian and Capricorn plates relative to the Somalian Plate for 20 distinct points in time since 20 Ma. The data are further used to place limits on the locations of the northern edge of the rigid Capricorn Plate and of the southern edge of the rigid Indian Plate along the Central Indian ridge. Data south of and including fracture zone N (the fracture zone immediately south of the Vema fracture zone), which intersects the Central Indian ridge near 10°S, are well fit assuming rigid Capricorn and Somalian plates, while data north of fracture zone N are not, in agreement with prior results. Data north of fracture zone H, which intersects the Central Indian ridge near 3.2°S, are well fit assuming rigid Indian and Somalian plates, while data south of and including fracture zone H are not, resulting in a smaller rigid Indian Plate and a wider diffuse oceanic plate boundary than found before. The data are consistent with Capricorn–Somalia motion about a fixed pole since ≈8 Ma, but require rotation about a pole 15° farther away from the Central Indian ridge from 20 to ≈8 Ma. The post-8-Ma pole also indicates Capricorn–Somalia displacement directions that are 7° clockwise of those indicated by the pre-8-Ma stage pole. In contrast, India–Somalia anomaly and fracture crossings are well fit by a single fixed pole of rotation for the past 20 Ma. India–Somalia motion has changed little during the past 20 Myr. Nonetheless, astronomically calibrated ages for reversals younger than 12.9 Ma allow resolution of the following small but significant changes in spreading rate: India–Somalia spreading slowed from 31 to 28 mm yr^{-1} near 7.9 Ma and later sped up to 31 mm yr^{-1} near 3.6 Ma; Capricorn–Somalia spreading slowed from 40 to 36 mm yr^{-1} near 11.0 Ma, later sped up to 38 mm yr^{-1} near 5.1 Ma and further sped up to 40 mm yr^{-1} near 2.6 Ma. The motion between the Indian and Capricorn plates is estimated by differencing India–Somalia and Capricorn–Somalia rotations, which differ significantly for all 20 pairs of reconstructions. India has rotated relative to the Capricorn Plate since at least ≈20 Ma. If about a pole located near 4°S, 75°E, the rate of rotation was slow, $0.11° \pm 0.01°$ Myr^{-1} (95 per cent confidence limits), from 20 to 8 Ma, but increased to $0.28° \pm 0.01°$ Myr^{-1} (95 per cent confidence limits) at ≈8 Ma. The onset of more rapid rotation coincides, within uncertainty, with the inferred onset at 7–8 Ma of widespread thrust faulting in the Central Indian basin, and with the hypothesized attainment of maximum elevation and initiation of collapse of the Tibetan plateau at ≈8 Ma. The plate kinematic data are consistent with steady India–Capricorn motion since 8 Ma and provide no evidence for previously hypothesized episodic motions during that interval. The convergence since 8 Ma between the Indian and Capricorn plates significantly exceeds (by 13 to 20 km) the convergence estimated from three north–south marine seismic profiles in the Central Indian basin. Where and how the additional convergence was accommodated is unclear.

Key words: crustal deformation, diffuse oceanic plate boundaries, India–Eurasia collision, plate tectonics, seafloor spreading, tectonics.

GJI Tectonics and geodynamics

1 INTRODUCTION

A broad region of deforming oceanic lithosphere that lies between the Central Indian ridge and the Sumatra trench in the equatorial Indian ocean acts as a diffuse oceanic plate boundary that separates the Indian Plate (to the north) from the Capricorn Plate (to the south) (Wiens *et al.* 1985; Gordon *et al.* 1990; Royer & Chang 1991; DeMets *et al.* 1994; Royer *et al.* 1997). These two plates are part of the larger Indo-Australian composite plate, which comprises the Indian, Capricorn, Australian and Macquarie component plates and multiple diffuse plate boundaries (Royer & Gordon 1997; Gordon 1998, 2000; Cande & Stock 2004). The pole of rotation between the Indian and Capricorn plates is well established as lying in the middle of the diffuse plate boundary, with the plates converging east of and diverging west of about 75°E over at least the past few million years (Gordon *et al.* 1990; DeMets *et al.* 1994; Royer *et al.* 1997; Gordon *et al.* 1998). The pole of rotation, determined solely from magnetic anomaly profiles and transform fault or fracture zone topography (and gravity signature) along the Central Indian and Carlsberg ridges, agrees excellently with independent data that indicate the sense of deformation in the diffuse oceanic plate boundary. Deformation in the converging part of the boundary is accommodated by thrust- and strike-slip faulting, whereas deformation in the diverging part is accommodated by normal- and strike-slip faulting, as indicated by the current pattern of earthquake mechanisms (Fig. 1). Moreover, the sediment of the Bengal fan, which overlies a large portion of the convergent part of the boundary, provides a medium in which thrust faulting and folding have been imaged on many seismic profiles (Eittreim & Ewing 1972; Moore *et al.* 1974; Weissel *et al.* 1980; Curray & Munasinghe 1989; Chamot-Rooke *et al.* 1993; Van Orman *et al.* 1995). In places the thrust faults can be seen to continue into the crust. Displacement rates and strain rates in this zone are the highest known for any purely oceanic diffuse plate boundary and make this region the first choice in investigating the processes occurring in such boundaries.

The histories of the motions of the plates that bound the zone are of interest for many reasons. The history of motion between the Indian and Capricorn component plates can inform us about the processes of deformation in the diffuse oceanic plate boundary and provide clues about the origin of the large-scale forces and torques responsible for the deformation. Such motion can be estimated only crudely from data from the diffuse plate boundary itself as there are no mid-ocean ridges or transform faults that separate the Indian and Capricorn plates. Such motion can only be accurately estimated indirectly, by first estimating the motion of India relative to Somalia and the motion of Capricorn relative to Somalia, and then differencing these two estimates. The history of India–Somalia and India–Capricorn motion also contains information about the timing, processes and forces involved in the India–Capricorn diffuse oceanic plate boundary that is not necessarily present or easily discerned from only the history of India–Capricorn motion.

The timing of onset of deformation in the India–Capricorn diffuse oceanic plate boundary has traditionally been dated through a combination of seismic stratigraphy and deep sea drilling in the Bengal fan. There is a regional unconformity, which in places is clearly related to the local onset of deformation and which has been dated by deep sea drilling in two locations as 7.5 to 8 Ma in age (Moore *et al.* 1974; Weissel *et al.* 1980; Curray & Munasinghe 1989; Cochran *et al.* 1990). This has led many prior workers to conclude that deformation and hence motion between the Indian and Capricorn plates commenced between 7.5 and 8 Ma. This timing can be independently tested through plate reconstructions, which
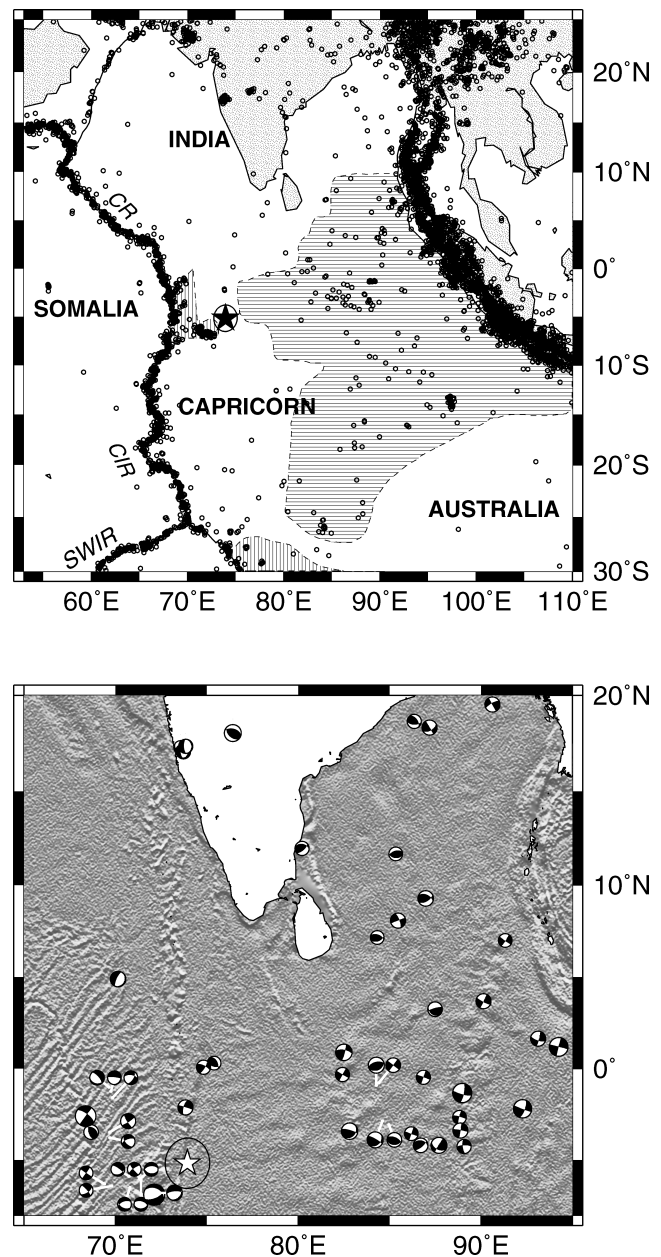

Figure 1. Upper panel: location map, regional plate geometry and epicentres of earthquakes with foci shallower than 60 km depth from 1963 to 2004. Star shows location of the India–Capricorn pole of rotation since 10.9 Ma and its 2-D 1σ confidence ellipse (Royer *et al.* 1997). Vertically striped regions are boundaries that accommodate distributed divergence; horizontally striped regions show boundaries that accommodate distributed convergence. Abbreviations: CR, Carlsberg ridge; CIR, Central Indian ridge; SWIR, Southwest Indian ridge. Lower panel: 1-min marine gravity field (Sandwell & Smith 1997) and earthquake focal mechanisms from the Harvard centroid moment tensor catalogue (1976–2004) and from other sources (see DeMets *et al.* 1994).

surprisingly indicate that motion between the Indian and Capricorn plates had initiated before 11 Ma, and perhaps much earlier (Gordon *et al.* 1998). A more detailed analysis of the history of motion between the Indian, Capricorn and Somalian plates may provide further information to illuminate these partly conflicting results.

The motion of India relative to Somalia is also a key link in determining the boundary conditions on the India–Eurasia collision. The

history of motion between India and Eurasia must be estimated indirectly through a plate motion circuit of India to Somalia to Antarctica to Nubia to North America to Eurasia. The motion between India and Somalia is the most important link in this circuit for two reasons. First, the motion between India and Somalia is the fastest of any of these plate pairs and thus resolvable changes in motion between this plate pair are potentially larger in magnitude than the comparable fractional changes in the motion between any other plate pair. Secondly, if there are changes over time in the torque that India and Eurasia exert on one another, it seems more likely that the smaller Indian Plate would have a larger change in motion than the larger Eurasian Plate in response to such changes in torque. If so, such changes are likely to be recorded in the history of the motion of India relative to Somalia.

The India–Eurasia collision, including the history of growth and uplift of the Tibetan plateau, on the one hand, and the deformation accommodating motion between the Indian and Capricorn plates on the other, are each worthy of investigation in their own right. Such investigations are all the more interesting, however, because the two deforming zones may be dynamically and causally linked. For example, Harrison *et al.* (1992) concluded that the Tibetan plateau reached its maximum elevation at approximately 8 Ma and suggested a causal link with the deformation in the equatorial Indian ocean, which was then believed to have commenced at the same time. Molnar *et al.* (1993) suggested a specific causal link, that the maximum elevation of the Tibetan plateau also came with a maximum outward push that increased the force per unit length that the Tibetan plateau and India apply to each other to a level exceeding the breaking strength of the oceanic lithosphere of the equatorial Indian ocean. These conjectures can be more specifically investigated from a more detailed history of the relative motions of the Indian, Capricorn and Somalian plates.

Independently of plate reconstructions, marine seismic profiles and sediment cores from Deep Sea Drilling Project site 218 and Ocean Drilling Project sites 717–719 have been used to establish that the cumulative north-to-south shortening accommodated by faulting across the Central Indian basin increases from west to east (Chamot-Rooke *et al.* 1993; Jestin 1994; Van Orman *et al.* 1995), in qualitative accord with the predictions of plate kinematic models. Moreover, it has been shown that the oldest of the regional seismic unconformities has an age of 8–7.5 Ma, interpreted by many as marking the onset of India–Capricorn deformation (Moore *et al.* 1974; Weissel *et al.* 1980; Curray & Munasinghe 1989; Cochran *et al.* 1990). Krishna *et al.* (2001) additionally report evidence for distinct phases of folding at 8.0–7.5, 5.0–4.0 and 0.8 Ma.

Here, we draw from thousands of airborne, shipboard and satellite crossings of magnetic lineations and fracture zones flanking the Central Indian and Carlsberg ridges to estimate rotations that describe India–Capricorn–Somalia relative motions at 20 points in time since 20.1 Ma. We use the new, detailed history of motion to set the stage for future, more detailed models of India–Eurasia motion and to investigate the following questions.

(i) What is the southern limit of the rigid Indian component plate and the northern limit of the rigid Capricorn component plate along the Central Indian ridge?

(ii) Have India–Somalia and Capricorn–Somalia motions changed significantly since 20 Ma?

(iii) If so, did the changes coincide with the onset at 8–7.5 Ma of thrust faulting at sites within the diffuse oceanic India–Capricorn plate boundary?

(iv) Does India–Capricorn convergence over the past $\approx$8 Ma agree with published convergence estimates from marine seismic profiles?

(v) Did India–Capricorn motion begin at $\approx$8 Ma, and is there any kinematic evidence for changes in post-8 Ma India–Capricorn–Somalia motion that correspond to three phases of folding during this interval as suggested by a recent re-analysis of marine seismic profiles from this region (Krishna *et al.* 2001)?

In evaluating statistical differences, we use the 95 per cent confidence level, which is equivalent to a 5 per cent level of significance, as the confidence level is 1 (or 100 per cent) minus the significance level. In some cases, a result may lie just outside or inside the threshold for 95 per cent confidence and, in other cases, well outside or inside the threshold. To convey additional information about how widely or narrowly a null hypothesis passed or failed, we also quote, usually parenthetically, the value of p, which is the probability of obtaining data as different or more different from the null hypothesis as the data we use. Barring bad luck, the smaller the value of p, the less likely that the null hypothesis is true.

2 DATA REDUCTION AND UNCERTAINTIES

We estimate India–Somalia and Capricorn–Somalia rotations using surface magnetic and aeromagnetic crossings of anomalies resulting from seafloor spreading and using satellite altimetric crossings of oceanic fracture zones flanking the Central Indian and Carlsberg ridges. Magnetic lineations were correlated for 20 isochrons (Table 1 and Fig. 2) out to the old edge of magnetic anomaly 6. Of the magnetic anomaly and fracture zone crossings we ultimately identified from the digital and analogue data available to us (Appendix, Figs A1–A7), we used 2232 magnetic anomaly crossings and 793 fracture zone crossings (Fig. 3) to constrain India–Somalia

Table 1. Magnetic anomaly ages.

Chron	Cande & Kent (1995)	APTS
1	0.78	0.78[1]
2	1.86	1.863[1]
2An.1y	2.580	2.582[1]
2An.3o	3.580	3.596[1]
3n.4	5.105	5.117[1]
3An.1y	5.894	6.040[2]
3An.2o	6.567	6.710[2]
4n.2	7.860	7.903[1]
4A	8.862	8.912[1]
5n.1y	9.740	‡
5n.2o	10.949	11.030[3]
5An.2o	12.401	12.447[3]
5AD	14.395	‡
5Bn.2	15.095	‡
5Cn.1y	16.014	‡
5Cn.3o	16.726	‡
5D	17.446	‡
5Ey	18.281	‡
6ny	19.048	‡
6no	20.131	‡

Ages are in millions of years before present and correspond to the tie points shown in Fig. 2. Reversal nomenclature is from Cande & Kent (1992). Chron designators followed by a y or o respectively indicate the young or old edge of the chron. APTS are astronomically calibrated ages. Sources: (1) Hilgen *et al.* (1995), (2) Krijgsman *et al.* (1999), (3) Abdul Aziz *et al.* (2003). ‡ indicates that no astronomically calibrated age is available.
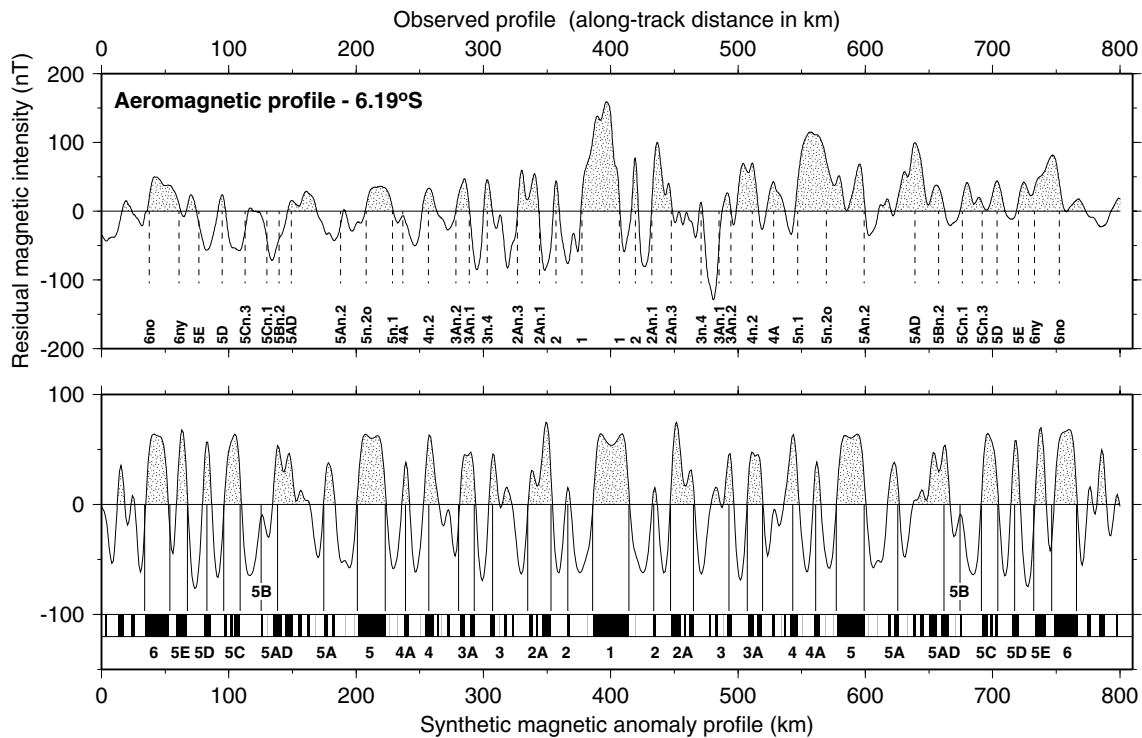
Figure 2. Magnetic reversals correlated for this study. The upper panel shows a typical aeromagnetic profile after reduction to the pole. The lower panel shows a synthetic magnetic profile computed using a 36 mm yr^{-1} spreading rate, a reversal transition width of 1.5 km, a source layer thickness of 0.5 km and a height above the source layer of 3.0 km. Vertical lines designate the precise locations selected for the reversal correlations.

and Capricorn–Somalia rotations. Table 2 summarizes the number of anomaly and fracture zone crossings used to estimate the best-fitting plate rotations for each isochron, as well as the number of magnetic anomaly segments and fracture zone segments that are needed to fit the data.

2.1 Magnetic anomaly crossings and their uncertainties

Magnetic anomaly crossings were identified from various sources, including various analogue data (detailed below) and more than 100 shipboard and aeromagnetic surveys. All digital magnetic profiles were reduced to the pole (Schouten & McCamy 1972) to facilitate correlation of the magnetic anomalies, which undergo a phase shift of ≈170° from the northwest end of the Carlsberg ridge to the southern end of the Central Indian ridge. DeMets *et al.* (1994) and Royer *et al.* (1997) describe the procedures we used in our reduction of the magnetic data.

Of the ≈3900 anomaly crossings we identified for the 20 isochrons shown in Fig. 2, ≈90 per cent are from digital shipboard and aeromagnetic data archived at the US National Geophysical Data Center and at various French institutions. The remaining crossings are from analogue profiles or maps published by Fisher *et al.* (1971), Karasik *et al.* (1986), Chaubey *et al.* (1990, 1993) and Ramana *et al.* (1993) or were provided by Dyment (private communication, 1996) for various cruises for which the digital data were unavailable to us (Tisseau 1978; Patriat 1987; Dyment 1991). The geographic distribution of the anomaly correlations close a gap between 19°S and 5°N in older data sets (e.g. Patriat 1987; Molnar *et al.* 1988; Royer & Chang 1991). Our data set is weakest northwest of ≈62°E along the Carlsberg ridge, where slow spreading rates and sparse shipboard and airplane coverage complicate efforts to identify anomalies. Various Russian cruises have mapped this region in

great detail (Glebovsky *et al.* 1995), but these data are unavailable to us.

Ultimately only 2232 of the ≈3900 magnetic anomaly crossings were used to estimate India–Somalia and Capricorn–Somalia rotations (Fig. 3). Most exclusions were of crossings that lie between fracture zones H and N, which are the limits to the diffuse oceanic plate boundary on the Indo-Capricorn side of the Central Indian ridge, as is discussed further below. Some other magnetic anomaly crossings could not be used because there were not enough crossings per segment (at least two anomaly crossings from one side of the ridge and at least one from the other) to be used to estimate a rotation.

Uncertainties in the locations of magnetic anomaly crossings are inferred from the dispersion of the data about the best-fitting model. The precision parameter, $\hat{\kappa}$, is inversely proportional to the variance of the data. $\hat{\kappa}$ equals $(N-m)/\chi^2$, where N is the number of data, m is the number of parameters used to fit the data and χ^2 is the normalized least-squares fit for the set of parameters that best fit the data (Royer & Chang 1991). If the assigned uncertainties reflect the random error in the locations of crossings, $\hat{\kappa}$ is expected to approximately equal 1. Values greater than 1 indicate that the dispersion is smaller than the assigned uncertainty by a factor equal to the square root of $\hat{\kappa}$. Anomaly crossings were initially assigned navigation-dependent uncertainties of ±3.0, ±3.2, ±3.9, or ±5.2 km (Royer *et al.* 1997). Preliminary inversions of the anomaly crossings for each of the 20 isochrons, with India–Somalia and Capricorn–Somalia data sets treated separately, gave values of $\hat{\kappa}$ ranging from 1.1 to 14.7 (Table 2). The initially assigned uncertainties thus exceed the standard deviations of the data by factors of 1.05 to 3.8. Ninety five per cent of the 2232 residual distances for anomaly crossings are smaller than 3.7 km and only four residual distances exceed 10 km. We chose to rescale the preliminary anomaly uncertainties for each of the
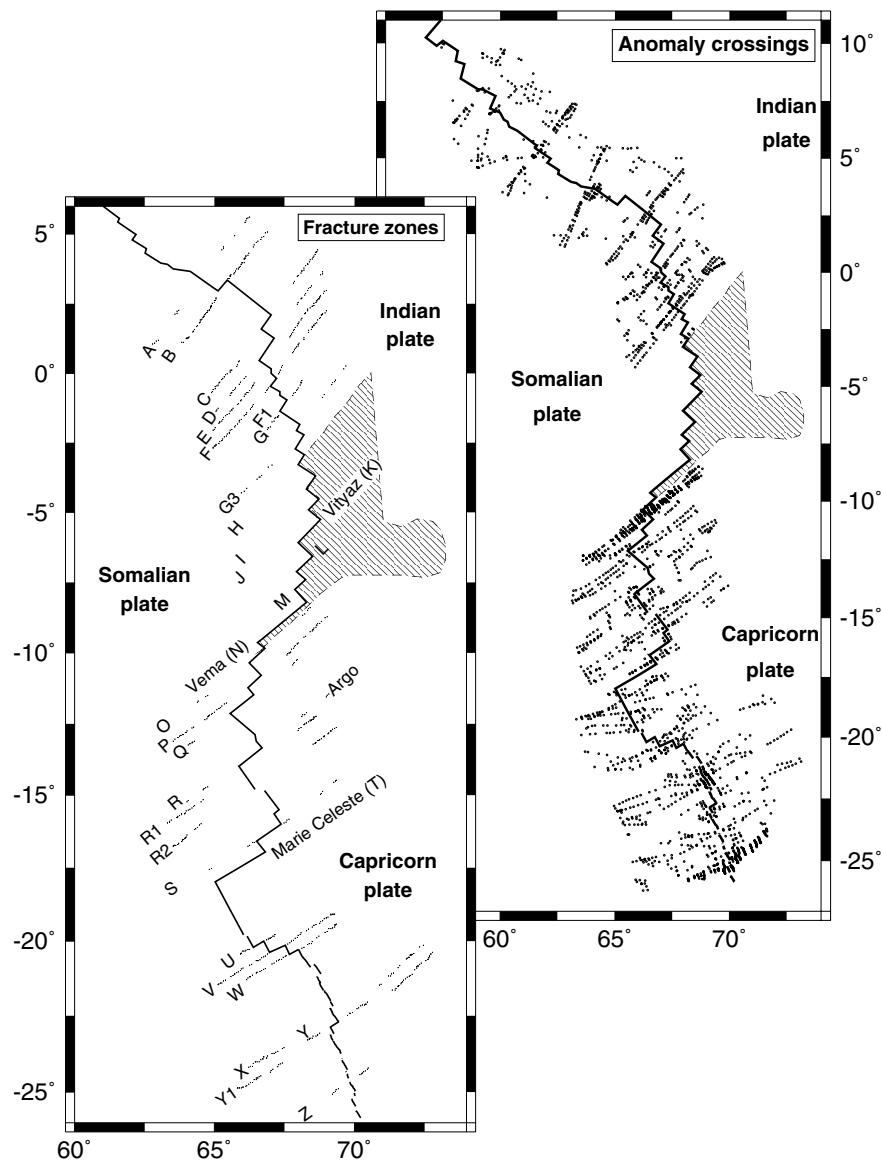
Figure 3. Locations of magnetic anomaly and fracture zone crossings used to estimate rotations between the Indian and Somalian plates (i.e. crossings north of 5°S) and between the Capricorn and Somalian plates (i.e. crossings south of 8°S). Labels A, B, C, etc. and F1, G3, R1 etc. are informal names of fracture zones (Royer *et al.* 1997). Diagonally ruled areas indicate the approximate extent of the zone accommodating divergent motion between the Indian and Capricorn plates. Detailed maps of all of the magnetic anomaly and fracture zone crossings identified for this study are presented in Figs A2–A7.

40 data subsets such that the associated value of $\hat{\kappa}$ for those crossings equals 1, which neglects the effects of any systematic errors.

2.2 Fracture zone crossings and their uncertainties

Because bathymetric soundings of the many fracture zones that offset the Central Indian and Carlsberg ridges are typically sparse, we used the 2-min global marine gravity grid estimated from Geosat and ERS-1 satellite altimetry (Sandwell & Smith 1997) to estimate the locations of fracture zone troughs (Figs A2–A7). Wavelengths shorter than 100 km in the marine gravity field largely reflect the uncompensated topography of the ocean floor (Sandwell 1984) and are thus well suited to this purpose.

We initially extracted crossings of fracture zone troughs using an automated routine to select all gridded gravity values within 5 km of the fracture zones flanking the Central Indian and Carlsberg ridges. Only grid cells with gravity values constrained by one or more satellite observations were selected. From the ≈10-km-wide swath of gravity values along each fracture zone, we constructed fracture zone perpendicular profiles at 3 km intervals along each fracture zone and for each profile identified the lowest gravity value as a proxy for the deepest part of the fracture zone valley. The procedure worked well except near ridge–transform intersections, where the gravity low associated with the axial valley locally deflects the linear gravity low associated with the fracture zone valley. Where this problem occurred, we removed the affected crossings.

This procedure resulted in more than 6000 crossings of the 34 fracture zones that offset the Central Indian and Carlsberg ridges (Figs. A2–A7), from which we extracted a subset (2545) to represent conjugate fracture zone segments for each of the 20 chrons. We excluded crossings of the large-offset fracture zones N and T (the Vema and Marie Celeste fracture zones) and of fracture zones H

Table 2. Somalia–Capricorn and Somalia–India data summary.

Chron	Somalia–Capricorn						Somalia-India					
	N_{anom}	m_{anom}	$\hat{\kappa}$	N_{fz}	m_{fz}	$\hat{\kappa}$	N_{anom}	m_{anom}	$\hat{\kappa}$	N_{fz}	m_{fz}	$\hat{\kappa}$
1	219	25	3.61	23	4	8.70	59	14	3.52	6	1	71.43
2	151	19	3.52	27	6	22.73	34	8	14.71	15	3	100.0
2An.1	137	21	4.31	27	5	10.42	45	10	5.88	10	2	8.13
2An.3	110	18	6.17	13	3	6.33	34	7	7.52	12	2	14.29
3n.4	93	14	2.87	14	3	26.32	21	5	6.10	10	2	11.11
3An.1	86	18	3.38	12	3	16.13	20	6	12.05	15	2	22.73
3An.2	76	14	4.07	8	2	11.76	20	6	13.89	14	4	40.00
4n.2	75	14	5.81	14	3	10.53	26	7	5.71	16	3	8.47
4A	70	11	2.90	13	3	7.14	33	8	3.10	15	3	20.00
5n.1	45	8	2.24	13	3	27.78	23	6	3.11	14	3	11.49
5n.2o	95	13	1.13	53	7	6.71	59	12	2.19	31	7	6.99
5An.2	55	11	1.56	32	6	7.35	50	11	2.09	21	7	8.62
5AD	39	9	1.49	42	7	7.19	34	8	3.13	24	6	5.21
5Bn.2	32	8	1.23	23	4	7.41	42	9	2.25	26	6	9.26
5Cn.1	36	6	2.92	29	6	6.33	31	7	7.46	24	6	6.58
5Cn.3	45	8	3.22	24	4	17.86	39	8	4.27	16	5	5.26
5D	46	8	2.42	22	5	4.93	34	8	4.83	16	3	19.61
5E	46	9	2.42	23	4	3.61	29	7	6.02	17	3	16.95
6ny	44	8	1.72	18	4	9.52	19	4	1.03	24	5	7.87
6no	47	8	2.99	8	2	200.0	33	9	2.62	29	5	8.20

N_{anom} and N_{fz} respectively are the numbers of magnetic anomaly crossings and fracture zone crossings that are used to estimate finite rotations for a given reconstruction. m_{anom} and m_{fz} respectively are the assumed numbers of palaeoridge segments and assumed number of fracture zone segments. Values of $\hat{\kappa}$ for anomaly crossings are estimated from the least-squares misfit to those anomaly crossings when they are inverted with crossings from a single fracture zone. Values of $\hat{\kappa}$ for fracture zone crossings are estimated from the least-squares misfit to those fracture zone crossings when they are inverted with anomaly crossings from a single spreading segment. The initial uncertainties assigned to the anomaly crossings are the same as those described by Royer *et al.* (1997). Values of $\hat{\kappa}$ for the anomaly crossings for each plate pair and time interval were used to reweight the anomaly uncertainties so that the $\hat{\kappa}$ for anomaly crossings for that reconstruction is unity.

to M, which are located in the zone of distributed India–Capricorn deformation, as discussed further below. Fracture zones, unlike magnetic isochrons, do not represent a palaeoplate boundary at any specific point in time, but instead integrate the boundary location over millions or tens of millions of years. Thus, they may degrade the resolution of a plate reconstruction if weighted too heavily relative to magnetic anomaly crossings, which are isochrons. For this reason, we chose to decimate the original, closely spaced set of crossings by a factor of 2 to avoid overweighting the fracture zone crossings relative to the less numerous anomaly crossings. The spacing between the crossings used to constrain any given rotation averages 8 ± 2 km.

Because of the close spacing of the isochrons used in the reconstructions (10 to 40 km on each side of the ridge), the rotations for adjacent isochrons are typically estimated from some of the same fracture zone crossings, even after the fracture zone crossings had been decimated as described above. Of the 793 fracture zone crossings we use, 87 (11 per cent) are used to estimate rotations for two or at most three adjacent isochrons. The fracture zone perpendicular components of displacement indicated by the best-fitting rotations described in later sections are thus weakly correlated from one isochron to the next and may result in estimated motions that are slightly smoother (in the fracture zone perpendicular direction) than if they were uncorrelated.

The subsediment axis of the Kane fracture zone (Atlantic ocean) lies within ≈ 10 km of the corresponding trough in gravity along 95 per cent of its length (Müller *et al.* 1991). This suggests that an appropriate 1σ uncertainty for a fracture zone crossing is ≈ 5 km, which we use herein. To compare the dispersion of the fracture zone crossings to this assigned uncertainty, we estimate rotations for each of the 20 sets of reconstructions using only the fracture zone crossings plus enough magnetic anomaly crossings from a

single segment to ensure convergence to a geologically reasonable reconstruction. This results in values of $\hat{\kappa}$ that range from 3.6 to 200.0 (Table 2), with an average of $\hat{\kappa} = 8.5$. The 5 km uncertainty we assigned to fracture zone crossings thus exceeds the random component of fracture zone uncertainties by an average factor of approximately 3. A comparison of rotations from crossings from only left-stepping or only right-stepping fracture zones suggests that systematic errors in fracture zone locations (such as a tendency for the inactive trace of the fault to lie closer to one side of the fracture zone valley) are 1 km or less. Thus, the ± 5.0 km uncertainty we assign to each fracture zone location may be conservative if systematic errors can be neglected.

For the best-fitting rotations described below, 99.6 per cent of the residual distances for the fracture zone crossings are less than their assigned uncertainty of 5 km, with a mean absolute misfit of 2.2 km.

3 METHODS AND ASSUMPTIONS

3.1 Estimating total rotations

We estimate best-fitting rotations using the fitting criterion of Hellinger (1979) applied to segments of magnetic anomaly crossings and segments of fracture zone crossings; we estimate the uncertainties of the rotations, described by covariance matrices, using the method of Chang (1988). Further details are given by Chang (1988) and Royer & Chang (1991).

3.2 Orthogonal component plots

Inspired by the use of orthogonal component plots in the interpretation of palaeomagnetic demagnetization data (Zijderveld 1967), Wilson (1993a) showed how to use such plots to display and to

interpret a time sequence of rotations. An ideal plot would display rotations and their uncertainties in a coordinate system for which the covariance between components vanishes. If the eigenvectors of all the covariance matrices of a time sequence of rotations were identical, then those eigenvectors would constitute an ideal set of basis vectors for the axes of the orthogonal components. In practice, the eigenvectors vary from rotation to rotation in a sequence but are nevertheless tightly grouped because their orientations are largely determined by the geometrical distribution of the crossings (Molnar & Stock 1985; Chang *et al.* 1990). The choice of coordinate axes parallel to the eigenvectors tend to decompose the rotations into three components, similar to those used by Wilson (1993a). The first component is evaluated parallel to the eigenvector having the largest eigenvalue and largest uncertainty, typically near the geographic mean of the location of the data. Its size (relative to the second component) is related to the distance of the pole of relative plate rotation from the geographic mean of the data locations, vanishing when the pole is 90° away and large when the pole is nearby or nearly antipodal (Wilson 1993a). The second component provides a measure of the average displacement parallel to the fracture zones, corresponding to the displacement between homologous magnetic anomalies on the two sides of a mid-ocean ridge. This eigenvector typically has the smallest eigenvalue (and uncertainty) and lies at 90° angular distance from the first eigenvector approximately along the great circle that contains both the first eigenvector and the pole of relative plate rotation. The third component measures displacement perpendicular to the fracture zones (zero if there is no change in the pole of relative plate rotation). The corresponding eigenvector is perpendicular to the first two eigenvectors.

During intervals of nearly constant motion, the ratio of any two of the three rotation components remains nearly constant. Ages in millions of years (i.e. absolute time) are not used; the results are thus unaffected by errors and uncertainties in the geomagnetic reversal timescale. Such plots are thus useful for detecting changes in plate motion (Wilson 1993a).

3.3 Assumed data segmentation

We sought to define the geometry of the palaeospreading centre for each isochron by requiring that the palaeoplate boundary consist of the fewest number of segments required to fit the data and that it evolve only slowly through time, if at all. The palaeogeometry was difficult to define in only two regions, along the Central Indian ridge south of fracture zone W and along the Carlsberg ridge northwest of fracture zone A. Axial discontinuities in the former region offset the present ridge axis (Parson *et al.* 1993; Briais 1995) and thus probably also offset the older, adjacent magnetic lineations. These discontinuities are readily apparent in the closely spaced crossings of the central anomaly, but are hard to define for older, more sparsely sampled anomalies. Along the northwestern half of the Carlsberg ridge, small palaeo-axial offsets and sparse anomaly crossings make it difficult to determine how many segments should be used to fit some groups of anomaly crossings. We experimented with alternative geometries along the northwestern Carlsberg ridge, but found that the resulting rotations are insensitive to a plausible range of palaeo-axial geometries. Further refinements to the palaeo-axial geometry will probably be needed once additional anomaly crossings become available for these regions.

3.4 Magnetic reversal ages

We use two geomagnetic polarity reversal timescales to estimate seafloor spreading rates and test for changes in plate motion. Cande

& Kent (1995) estimate the ages of magnetic reversals via interpolation between reversals that are presumably well dated radiometrically, subject to the condition that the interpolated anomaly ages result in smoothly varying spreading rates in the southern Atlantic. Hilgen *et al.* (1995), Krijgsman *et al.* (1999) and Abdul Aziz *et al.* (2003) collectively estimate the ages of nearly all reversals younger than 12.9 Ma by correlating sedimentary cycles in marine and lacustrine sections with variations in insolation at 65°N as predicted from Milankovitch forcing. The latter are expected to be approximately 2 orders of magnitude more accurate than the former; this expectation is given support by the spacing of magnetic anomalies across globally distributed spreading centres, which indicate smoother rates for the latter timescale than for the former (Wilson 1993b; Krijgsman *et al.* 1999; Abdul Aziz *et al.* 2003).

4 RESULTS

4.1 Intersection of the India–Capricorn diffuse plate boundary with the Central Indian ridge

Reconstructions of fracture zone crossings from the undeformed Somalia Plate using India–Somalia best-fitting rotations indicate a systematic misfit between rotated and fixed crossings for all fracture zones south of and including fracture zone H (Fig. 4). The misfit increases to the south and with increasing age, with most of the increase occurring for reconstructed points corresponding to the past ≈10 Myr. These results are consistent with distributed deformation that has persisted for 10 Myr or longer. Moreover, the results indicate that the near-ridge deforming region that accommodates India–Capricorn motion extends northwards to and includes fracture zone H. The $M_s = 7.6$ 2003 July 15 earthquake and related aftershocks along fracture zone H (Fig. 4) offer independent evidence for this conclusion. From these results, we assign all plate boundary segments to the northwest of fracture zone H to the India–Somalia plate pair. This is smaller, by a few hundred kilometres along strike of the Carlsberg ridge, than the India–Somalia boundary inferred by Royer *et al.* (1997) from analysis of crossings of magnetic anomaly 5 and associated fracture zones.

Reconstructions of magnetic anomaly and fracture zone crossings from the undeformed Somalia Plate using Capricorn–Somalia best-fitting rotations (Fig. 5) indicate a systematic misfit of rotated and fixed crossings beginning with the spreading segment immediately north of fracture zone O. The misfit increases to the north and with increasing age, again with most of the increase occurring for reconstructed points corresponding to the past ≈10 Myr. From these results, we assign all magnetic anomaly and fracture segments south of and including fracture zone O to the Capricorn–Somalia plate pair, identical to the geometry inferred by Royer *et al.* (1997) from analysis of crossings of magnetic anomaly 5 and associated fracture zones.

4.2 Capricorn–Somalia plate motion

Reconstructions of magnetic anomaly and fracture zone crossings from the Capricorn Plate onto the Somalia Plate (Fig. 6) using the best-fitting rotations from Table 3 illustrate the absence of major gaps in the data along the plate boundary for all isochrons considered here. Residual distances of the reconstructed crossings from their best-fitting great circle segments average 2.1 km for the 1547 magnetic anomaly crossings and 2.2 km for the 438 fracture zone crossings.
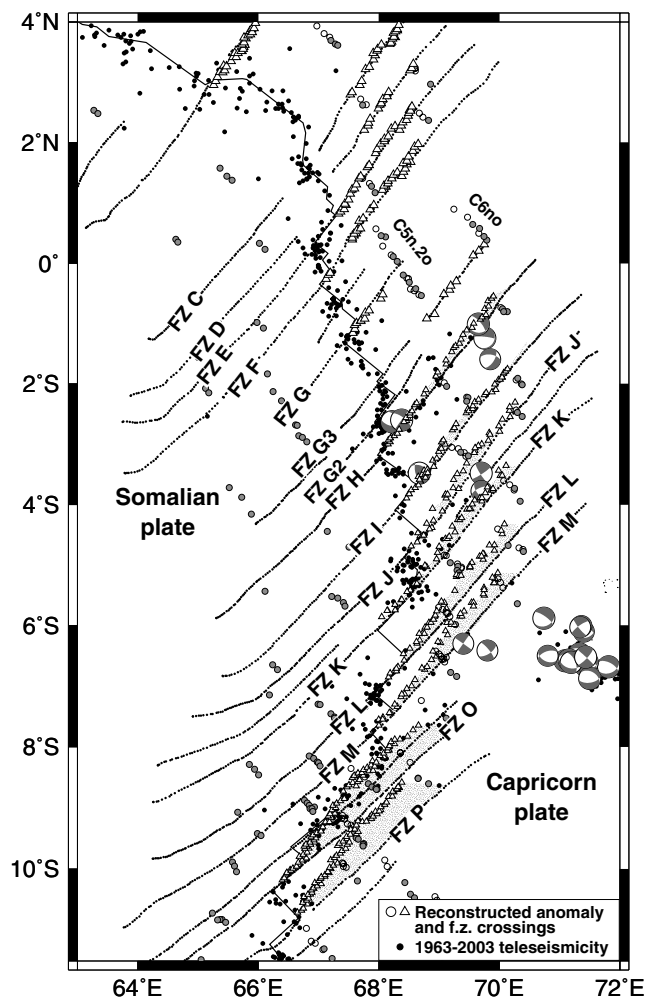
Figure 4. Search for the southeastern limit of the rigid Indian Plate near the Central Indian ridge. Open triangles show fracture zone crossings from the undeformed Somalia Plate after they have been reconstructed to their positions relative to the Indian Plate using best-fitting rotations from Table 3. The reconstructed crossings of fracture zones G and G3 coincide with the unrotated fracture zone traces northeast of the Carlsberg ridge. Thus, the Indian Plate is rigid (within uncertainties) at least as far southeast as fracture zone G3. Reconstructed crossings of fracture zone H lie systematically northwest of the unrotated fracture zone traces northeast of the Carlsberg ridge indicating that fracture zone H northeast of the Carlsberg ridge lies in the zone of deformation that accommodates motion between the Indian and Capricorn plates. The misalignment of the reconstructed fracture zone crossings relative to the unrotated fracture zone crossings, indicated by the shaded regions, increases with age, indicating that the displacement of the Indian Plate relative to the Capricorn Plate increases with age.

The Capricorn–Somalia rotation poles for the past 8 Ma (chron 4n.2) to 10 Ma (chron 5n.1) group near 12°N, 49°E (Fig. 7). Poles for older isochrons lie to the northwest of the cluster of young poles, with the poles for the oldest reconstructions tending to lie the farthest (near 17°N, 44°E) from the cluster of poles for the past 8–10 Ma. The observed, time-transgressive northwestward migration of the older finite rotation poles indicates that the Capricorn and Somalian plates rotated about a pole more distant from the plate boundary before 8–10 Ma. A simple estimate of the older stage pole is found by differencing the rotations for chrons 6no and 4n.2, giving an early stage rotation of 6.02° about a pole at 21.3°N, 37.2°E in the fixed Capricorn frame of reference; the pole is located at 22.3°N, 38.1°E
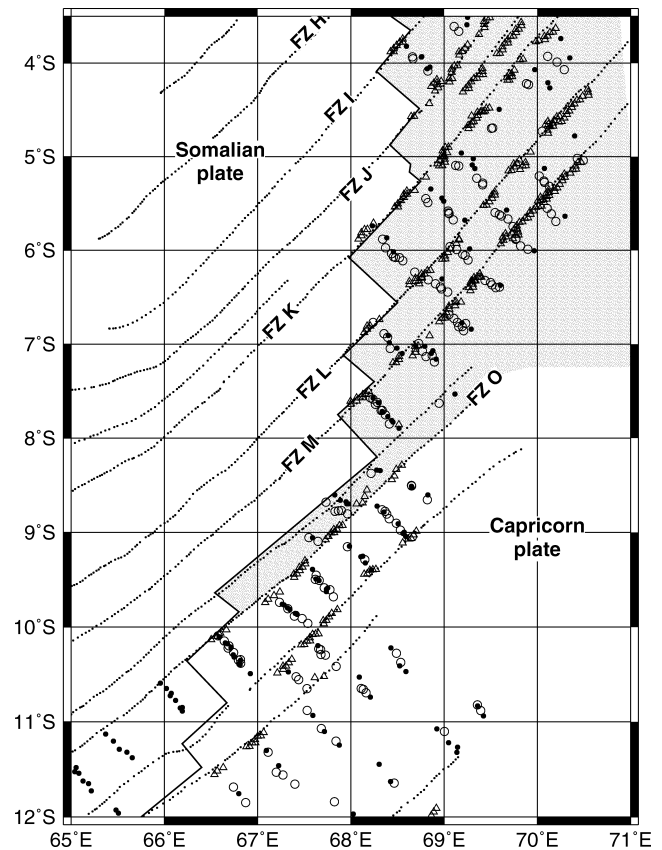

Figure 5. Search for the northern limit of the rigid Capricorn Plate near the Central Indian ridge. Open circles and triangles respectively show magnetic anomaly and fracture zone crossings from the undeformed Somalia Plate after they have been reconstructed to their positions relative to the Capricorn Plate using best-fitting rotations from Table 3. Filled circles show fixed magnetic anomaly crossings located northeast of the Central Indian ridge (either on the rigid Capricorn Plate or in the diffuse India–Capricorn plate boundary). Reconstructed crossings from the Somalian Plate agree well with their counterparts southeast and south of fracture zone O, but are systematically misfit northwest and north of fracture zone O. Thus, the Capricorn Plate is rigid (within uncertainties) southeast and south of fracture zone O, but Indo-Capricorn lithosphere northwest and north of fracture zone is part of the diffuse boundary between the Indian and Capricorn plates. The misalignment of the reconstructed magnetic anomaly crossings relative to the unrotated magnetic anomaly crossings increases with age, indicating that the displacement of the Indian Plate relative to the Capricorn Plate increases with age.

in the fixed Somalia frame of reference. The 20–8 Ma stage pole lies close to, but differs significantly from, the India–Somalia poles of rotation discussed below. This significant difference is evidence for additional relative motion between the Indian and Capricorn plates before 8 Ma (Gordon *et al.* 1998).

4.2.1 Orthogonal component plot

Whether and how long the Capricorn Plate rotated about an approximately fixed pole relative to the Somalian Plate is more readily examined in an orthogonal component plot (Fig. 8). If the plates have rotated about a single fixed pole for the past 20 Myr, the points in each plot would lie along a single straight line segment, which they do not (Fig. 8). If the plates have rotated about two successive fixed poles of rotation for the past 20 Myr, the points should lie
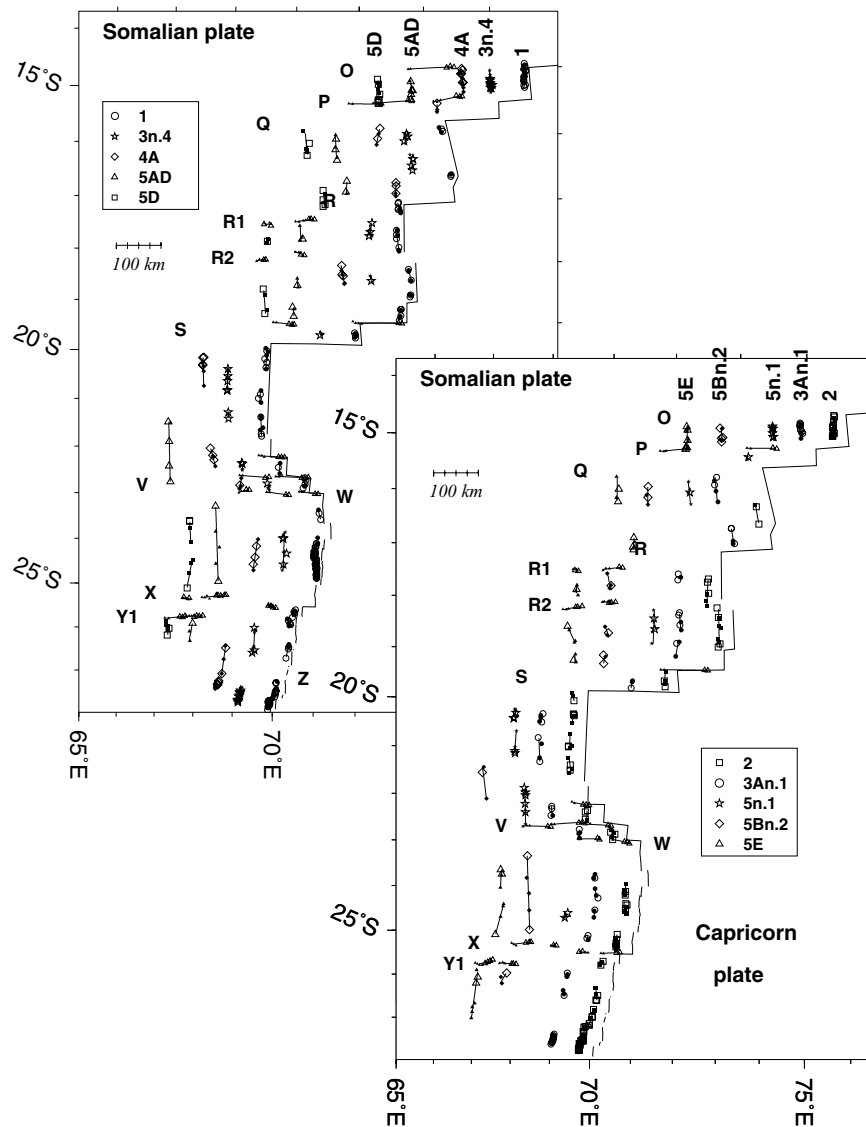
Figure 6. Anomaly and fracture zone crossings from the Capricorn Plate rotated onto the Somalian Plate using best-fitting rotations (Table 3). Solid and open symbols respectively show fixed and rotated data. Fracture zone crossings are shown with small triangles and align horizontally in the figure. Heavy lines show the present Central Indian ridge. All panels are oblique Mercator projections about the mean Capricorn–Somalia pole of rotation since 20 Ma.

along two different straight line segments that connect in the plot. Within uncertainties, the progression of ratios of Ω_{skew} to Ω_{mag} and of Ω_{fz} to Ω_{mag} are both consistent with such a two-stage-pole interpretation (Fig. 8), with an apparent change in motion at either chron 4n.2 (8 Ma) or chron 5n.1 (10 Ma). The change in the ratio of Ω_{skew} to Ω_{mag} corresponds to the stage pole lying 15° closer to the Central Indian ridge for reconstructions since 8–10 Ma than for those before 8–10 Ma. The change in the ratio of Ω_{fz} to Ω_{mag} corresponds to a 7° clockwise change in the displacement direction along the Capricorn–Somalia plate boundary at approximately 8–10 Ma and is several times smaller than the change in the ratio of Ω_{skew} to Ω_{mag}.

Thus, the orthogonal component plot shows that an important change in Capricorn–Somalia motion took place at 8–10 Ma. The larger change was that the pole of rotation moved approximately 15° closer to the Central Indian ridge, corresponding to an increase (or at least a relative increase) in the rate of rotation about an axis parallel to the eigenvector near the geographic mean of the data locations. Simultaneously, there was a lesser but significant 7° clockwise change (going forwards in time) in the direction of relative plate motion across the Central Indian ridge.

4.2.2 Displacement path analysis

We examine changes in Capricorn–Somalia displacement rates and directions along a displacement path that intersects the present plate boundary near the skew-fit eigenvector $\hat{\Omega}_{skew}$ (Fig. 9). Reconstruction uncertainties for points along this path are smaller than elsewhere along the plate boundary because the uncertainties in Ω_{skew}, which is the most uncertain of the three components of rotation, contribute little to the uncertainty in the reconstructed point locations. Changes in displacement rates and directions along this path thus illustrate changes in Ω_{mag} and Ω_{fz}, the rotation components that are respectively parallel to the magnetic anomaly fit eigenvector and the fracture zone fit eigenvector.

If the ratio of Ω_{fz} to Ω_{mag} has remained constant since chron 6no, all 21 points along the path shown in Fig. 9 would lie along a single small circle. We tested this hypothesis by finding the small circle that
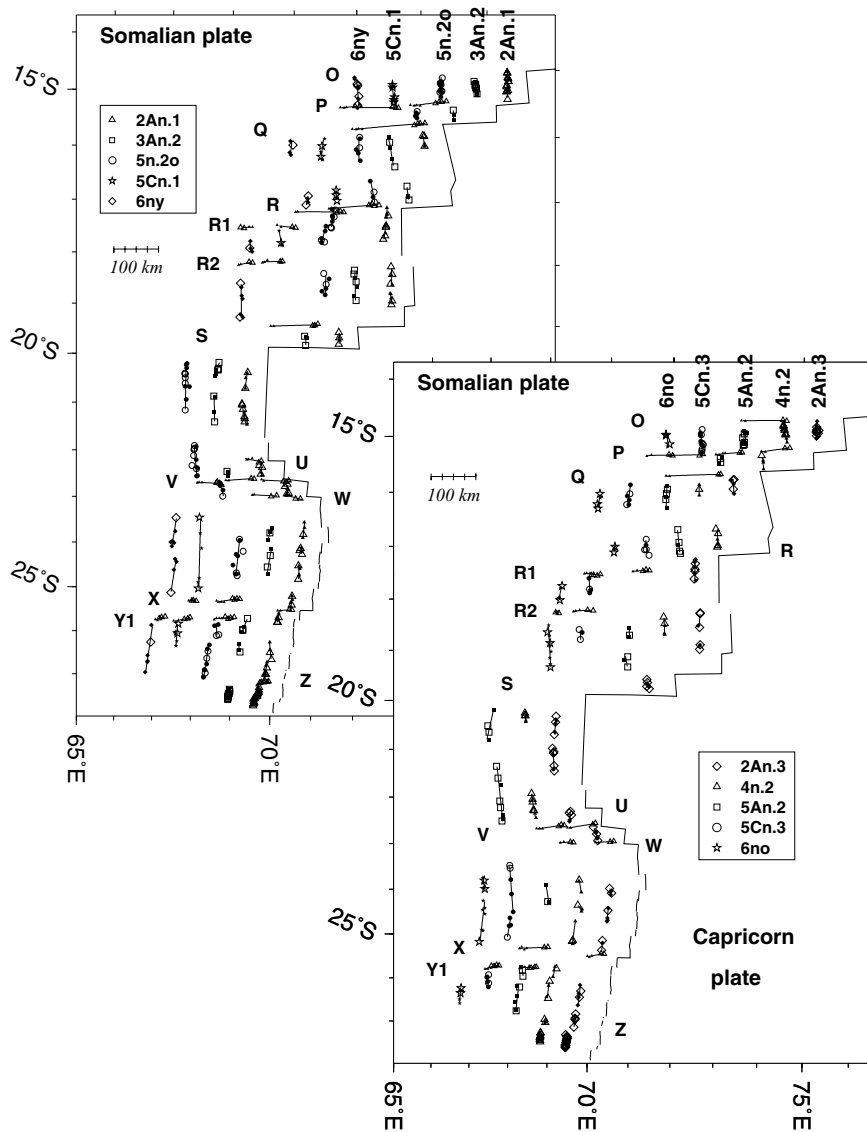
Figure 6. (*Continued.*)

minimizes the weighted least-squares misfit to the 21 reconstructed points. This best-fitting small circle has $\chi^2 = 211.2$ for 19 degrees of freedom, indicating that the reconstructed points are misfit on average by a factor of 3.3 times their uncertainties. If we instead fit the 21 points using two small circles, representing a different ratio of Ω_{fz} to Ω_{mag} from the present to chron 4n.2 than from chron 4A to chron 6no, $\chi^2 = 27.4$ for 17 degrees of freedom. The nine-fold improvement in the fit of the two small circle model relative to that of a single small circle model shows that the change at 8–10 Ma in the ratio of Ω_{fz} to Ω_{mag} (Fig. 8), corresponding to the 7° clockwise rotation of the displacement direction, is significant.

Whereas the plot of Ω_{skew} versus age indicates a change in slope near 8–10 Ma, the plot of Ω_{mag} versus age does not (Fig. 10). Thus, the 15° shift of the rotation stage pole towards the Central Indian ridge near 8–10 Ma, described above (Fig. 7), is the result mainly of a change in the rate of change of Ω_{skew}. We examined whether this change in pole location was accompanied by a change in seafloor spreading rates by using a reduced-distance plot (Fig. 11). Changes in slope correspond to changes in rate. We focus on the past 12.9 Myr, for which the timescale has been calibrated to

Milankovitch cycles (Abdul Aziz *et al.* 2003) and for which the 1σ uncertainties in reversal ages are $\approx$20 000 yr. Rates since 12.4 Ma indicate that spreading slowed from $\approx$41 to $\approx$35 mm yr^{-1} at 11 to 10 Ma, sped up to $\approx$38 mm yr^{-1} at 7 to 6 Ma and further sped up to $\approx$40 mm yr^{-1} at 2 to 3 Ma (Fig. 11). Nominal rates from 20 to 12.4 Ma are faster than those since 12.4 Ma, but spreading could have been as slow as 41 mm yr^{-1} or even slower within the relatively large uncertainties (1σ uncertainties of 1 to 2 Myr) in the geomagnetic reversal timescale for ages exceeding 12.9 Ma. In any event, any change in spreading rate at $\approx$8 Ma was modest; if any change occurred coevally with the change in pole position, it was a decrease in spreading rate of approximately 6 mm yr^{-1}.

4.2.3 Has the Capricorn–Somalia angular velocity remained constant since 8 Ma?

Given the evidence that stage spreading rates since 8 Ma increased from 35 to 38 mm yr^{-1} and then to 40 mm yr^{-1}, we next examine whether Capricorn–Somalia data are consistent with a constant rotation since 8 Ma or instead require one or more changes. We first
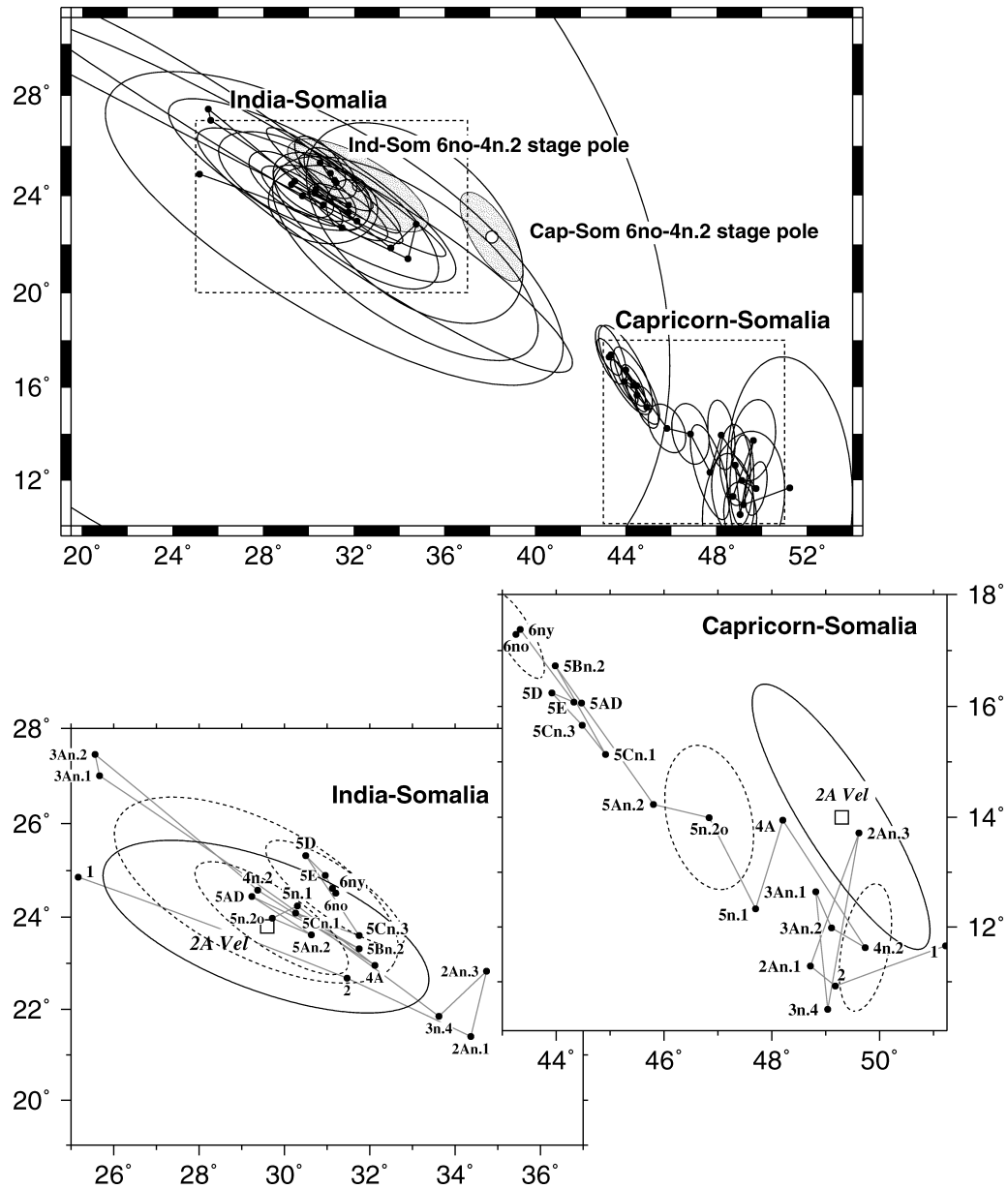
Figure 7. Locations and 2-D 95 per cent confidence regions for Capricorn–Somalia and India–Somalia poles of rotation (Table 3). The confidence regions are stippled for the India–Somalia and Capricorn–Somalia chron 6no to 4n.2 stage poles (shown in fixed Somalia coordinates). Dashed lines designate limits of the enlarged areas shown in the lower two panels. Representative confidence ellipses are shown in the lower two panels, as are the poles of rotation (squares labelled 2A vel) from estimates of India–Somalia and Capricorn–Somalia angular velocities averaged over the past 3 Myr (DeMets *et al.* 1994).

test whether the data for chrons 1no to 4n.2 are consistent with rotation about a fixed pole and, if so, whether they are consistent with a constant angular rotation rate.

A fixed pole with variable rates of rotation requires one set of pole coordinates and N rotation angles for N time steps, totaling $2 + N$ adjustable parameters. A constant rotation requires only three adjustable parameters, the pole coordinates and a rotation rate. Each best-fitting rotation is specified by a unique pole of rotation and angle, totaling $3N$ parameters for N rotations.

We constructed a fixed pole model in two steps. We first determined the Fisher mean location of the poles of the best-fitting rotations for chrons 1 to 4n.2 weighted by the angle of rotation. With the pole fixed to this location, the rotation angles for chrons 1 to 4n.2 were varied to solve for the angle that minimized the normalized

least-squares misfit to the data for each point in time. The summed least-squares misfit (i.e. χ^2) for the 1085 anomaly and fracture zone crossings for these eight sets of reconstructed data is 708.6, which exceeds by 29.2 the value of 679.4 for the eight best-fitting rotations, which use 14 additional parameters to fit the data. The difference in the least-squares fits is significant ($p = 0.01$). Repeating this test for different assumed locations for the fixed pole did not significantly improve the fit. A test for a fixed pole from the present to chron 3An.2 (6.6 Ma), however, shows no significant difference ($p = 0.09$) from the best-fitting model. Testing for a fixed pole since chron 4A (8.9 Ma) yields a substantially worse fit ($p = 4 \times 10^{-6}$) than the best-fitting model. We conclude that the data are consistent with Capricorn–Somalia rotation pole having been fixed since 6.6 Ma.
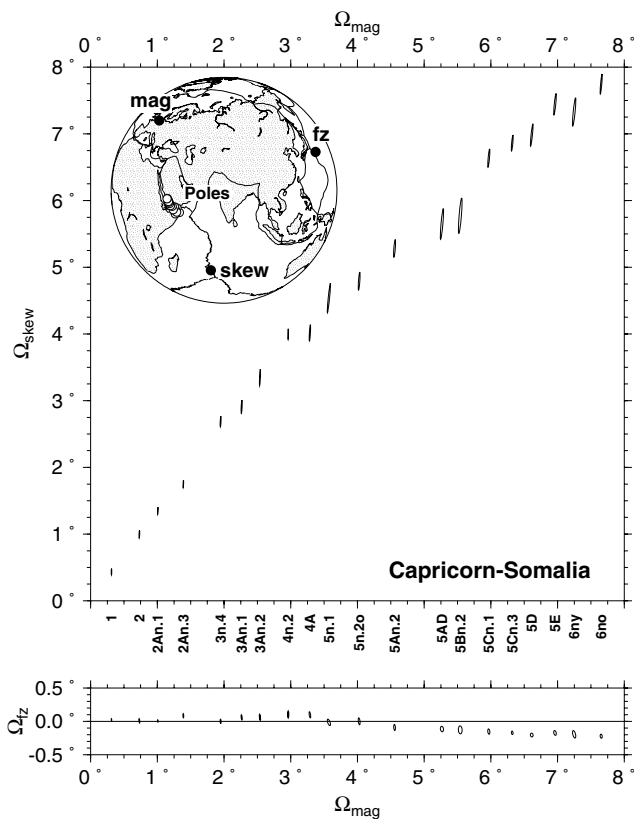
Figure 8. Orthogonal component plot of Capricorn–Somalia total rotations and 2-D 1σ error ellipses. Open circles on the inset globe show pole locations from Fig. 7. Ω_{skew}, Ω_{mag} and Ω_{fz} respectively are the components of rotation along the approximate locations of the skew misfit, magnetic anomaly misfit and fracture zone misfit eigenvectors, the locations of which are shown on the inset globe. The least uncertain component of rotation for the reconstructions is Ω_{mag}; its 1-D 1σ uncertainty averages 0.005°, corresponding to an average 1σ displacement uncertainty of 0.5 km. The most uncertain component of rotation is Ω_{skew}; its 1-D 1σ uncertainty averages 0.057°, corresponding to a 1σ displacement uncertainty as large as 1.1 km at the northern end of the plate boundary, decreasing to zero for points close to this nearby partial uncertainty rotation. The intermediate uncertainty is Ω_{fz}; its 1-D 1σ uncertainty averages 0.010° corresponding to an average 1σ displacement uncertainty of 1.1 km.

We tested for a constant rate of angular opening from 0 to 7.9 Ma by fitting a slope and intercept to the time-series of the corresponding eight rotation angles while the rotation is constrained to be about the fixed pole described above. Ages for the rotation angles were assigned from the astronomically calibrated reversal timescale (Table 1). Standard errors for the rotation angles were taken from the fixed-pole analysis. The best-fitting slope (0.617° Myr^{-1}) and intercept (0.067°) for the eight rotation angles results in $\chi^2 = 15.6$ assuming 1σ uncertainties in reversal ages of 20 000 yr. The misfit is significant ($p = 0.02$) for 6 degrees of freedom.

4.3 India–Somalia plate motion

Reconstructions of India–Somalia anomaly and fracture zone crossings (Fig. 12) using the best-fitting rotations from Table 3 give average misfits of 2.3 km for the 685 anomaly crossings and 2.2 km for the 355 fracture zone crossings, similar to those for the Capricorn–Somalia data (2.1 and 2.2 km, respectively). In contrast with the Capricorn–Somalia rotation poles, the India–Somalia rota-
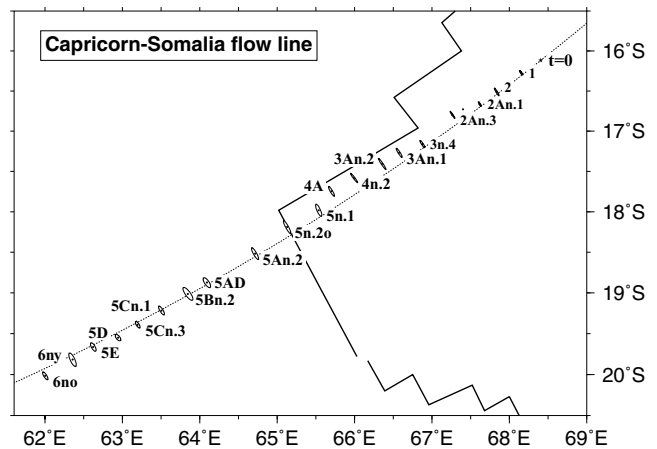

Figure 9. Displacement path of a point on the Capricorn Plate reconstructed relative to the Somalian Plate since C6no. The path originates at the old edge of anomaly 6 (solid star) on the Capricorn Plate and intersects the present boundary near its geographic centre. Capricorn–Somalia rotations and covariances (Table 3) are used to construct the path and 2-D 95 per cent confidence regions for rotated points. The dotted small circle is the one that best fits the reconstructed locations for C6no to the present.

tion poles do not indicate any change in location over the past 20 Myr (Fig. 7).

4.3.1 Orthogonal component plot

Given the pronounced change in the slope of Ω_{skew} versus Ω_{mag} for Capricorn–Somalia motion (Fig. 8), it is surprising that the same plot for India–Somalia motion shows no obvious change in slope and that the data lie nearly along a straight line, albeit with some dispersion (Fig. 13). Sixteen of the 20 points on the plot of Ω_{skew} versus Ω_{mag} for India–Somalia motion can be fit by a single straight line within their uncertainties (Fig. 13). The stage rotation that bests describes India–Somalia motion from 20.1 to 7.9 Ma (chron 6no to 4n.2) is 5.57° about a pole located at 24.4°N, 32.2°E in the fixed Somalia frame of reference and 24.5°N, 32.2°E in the fixed India frame of reference. These are located an insignificant 2.4° farther from the mean data location than is the chron 4n.2 pole. Thus, there is no evidence for a significant change in the India–Somalia pole at 8 Ma, in contrast to the 15° change in the Capricorn–Somalia stage pole.

4.3.2 Displacement path analysis

We reconstruct India–Somalia displacement rates and directions along a displacement path that intersects the present plate boundary near the average skew misfit eigenvector axis (Fig. 14). The reconstructed points are more dispersed than are their counterparts along the Capricorn–Somalia displacement path (Fig. 9). Any change in the ratio of Ω_{skew} to Ω_{mag} is evidently much smaller than for Capricorn–Somalia motion.

Changes in nominal India–Somalia seafloor spreading rates since chron 6no (Fig. 11) broadly resemble changes in Capricorn–Somalia spreading rates but differ in detail. Over the time interval calibrated to Milankovitch cycles, rates since 12.4 Ma indicate that spreading slowed from ≈33 to ≈28 mm yr^{-1} at approximately 8 Ma and sped up to ≈31 mm yr^{-1} at 4 to 3 Ma (Fig. 11). Nominal rates from 20 to 12.4 Ma are faster than those since 12.4 Ma, but spreading could have been as slow as 33 mm yr^{-1} or even slower within the
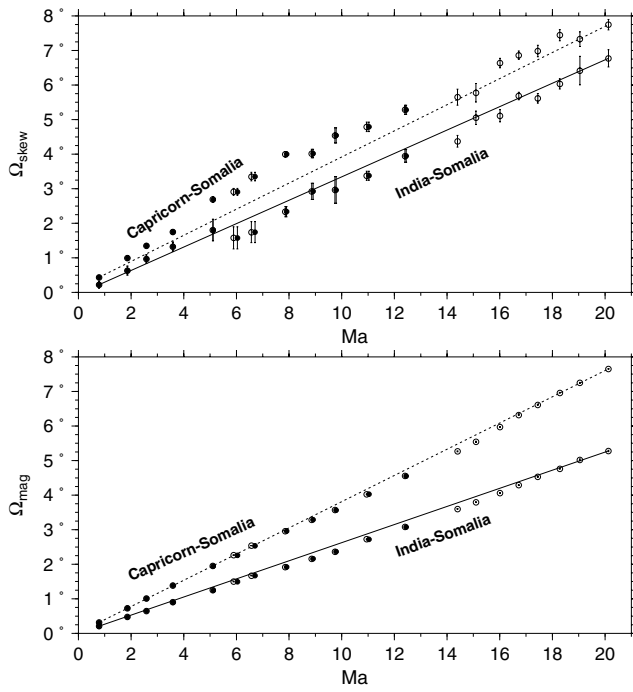
Figure 10. Plots of Ω_{skew} and Ω_{mag} versus age for both the Indian–Somalian and Capricorn–Somalian plate pairs. Straight reference lines connect the youngest and oldest point for each set of estimates. Both components of India–Somalia motion, as well as the Ω_{mag} component of Capricorn–Somalia motion, are approximately consistent with constant rates of rotation for the past 20 Myr. In contrast, the Ω_{skew} component of Capricorn–Somalia indicates relatively slower rotation before ≈8 Ma than since. Open and filled symbols are respectively determined from the Cande & Kent (1995) timescale and from the astronomically calibrated timescale (Table 1).

relatively large uncertainties (1σ uncertainties are 1 to 2 Myr) in the geomagnetic reversal timescale for ages exceeding 12.9 Ma.

The decrease in spreading rate of approximately 5 mm yr^{-1} near 8 Ma is the only significant indication of any change in India–Somalia motion near the time when many believe that the Tibetan plateau reached its maximum elevation.

4.3.3 Has the India–Somalia angular velocity remained constant since 20 Ma or since 7.9 Ma?

Following procedures described above, we test the hypotheses of a fixed pole for India–Somalia motion since 20 Ma and of a constant angular velocity since 7.9 Ma. For a pole of rotation fixed to the weighted Fisher mean location of the chron 1no to chron 6no rotation poles, varying the opening angles for each point in time to optimize the fit to the data results in a least-squares fit significantly worse than for the 20 best-fitting rotations ($\chi^2 = 404.6$ versus $\chi^2 = 463.6$), but not strongly so ($p = 0.02$). The data are thus inconsistent with the rotation pole having been perfectly fixed since 20 Ma, but only modest changes in its location are required by the data. For a pole of rotation fixed to the weighted Fisher mean location of the chron 1no to chron 4n.2 rotation poles, varying the opening angles for chrons 1no to 4n.2 to optimize the fit to the data results in a least-squares fit insignificantly worse ($p = 0.41$) than for the eight best-fitting rotations ($\chi^2 = 145.1$ versus $\chi^2 = 159.6$). Thus the data are consistent with the pole of rotation having been fixed for the past 7.9 Myr. Using astronomically calibrated reversal ages (Table 1) with assumed 1σ errors of ±0.02 Myr, as well as standard errors for
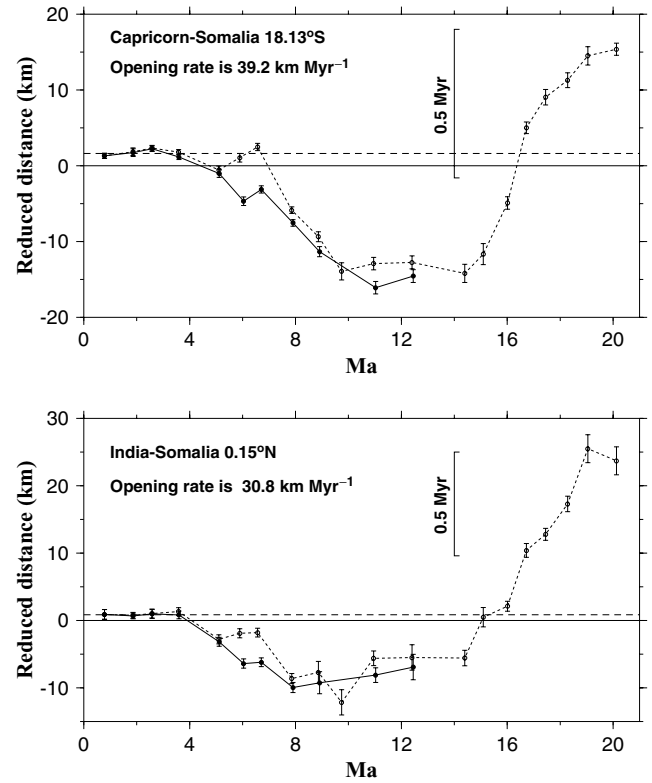
Figure 11. Reduced distance plots along reference paths. Filled circles: distances reduced using an astronomically calibrated timescale (Hilgen *et al.* 1995; Krijgsman *et al.* 1999; Abdul Aziz *et al.* 2003). Open circles: distances reduced using the timescale of Cande & Kent (1995). If the rate of opening was constant and if there were no errors in the timescale, the points would plot on a straight line. If the true rate equalled the reducing rate (labelled opening rate in the figure), the line would be horizontal. If the true rate were faster than the reducing rate, the line would slope up to the right; if the true rate is less than the reducing rate, the line would slope down to the right. The horizontal dashed lines are the best fits through the data for the past 4 Myr. The non-zero intercept of the horizontal lines is mainly the result of the systematic outward displacement of magnetic reversal boundaries away from the axis of spreading (Atwater & Mudie 1973; Klitgord *et al.* 1975). Here, the observed outward displacement is 1–2 km, similar to intercepts of 1 to 3 km found at other slow spreading centres (DeMets & Wilson, personal communication, 2004). The observed changes in slope of the sequence of reduced distances indicate changes in spreading or errors in the timescale or both. Whereas uncertainties in the astronomically calibrated timescale are approximately ±20 kyr, uncertainties in the Cande & Kent (1995) timescale are ±1 to ±2 Myr. A vertical bar shows how far the reduced distances shift for an error of 0.5 Myr in the timescale for ages exceeding ≈12 Ma.

the fixed-pole rotation angles from the fixed-pole analysis, linear regression of the opening angles results in a poor fit, with $\chi^2 = 29.8$ for 6 degrees of freedom ($p = 4 \times 10^{-5}$). Thus, the data are inconsistent with a constant opening rate over the past 8 Myr. The obvious explanation is the ≈3 mm yr^{-1} increase in spreading rate at 4 to 3 Ma noted above.

4.4 India–Capricorn plate motion

The India–Capricorn rotation for each point in time is first estimated by subtracting the best-fitting (i.e. unconstrained) Capricorn–Somalia rotation from the coeval best-fitting India–Somalia rotation (Table 4). Fifteen of the resulting 20 poles of India–Capricorn rotation are located between 73°E and 77°E with the other five nearby
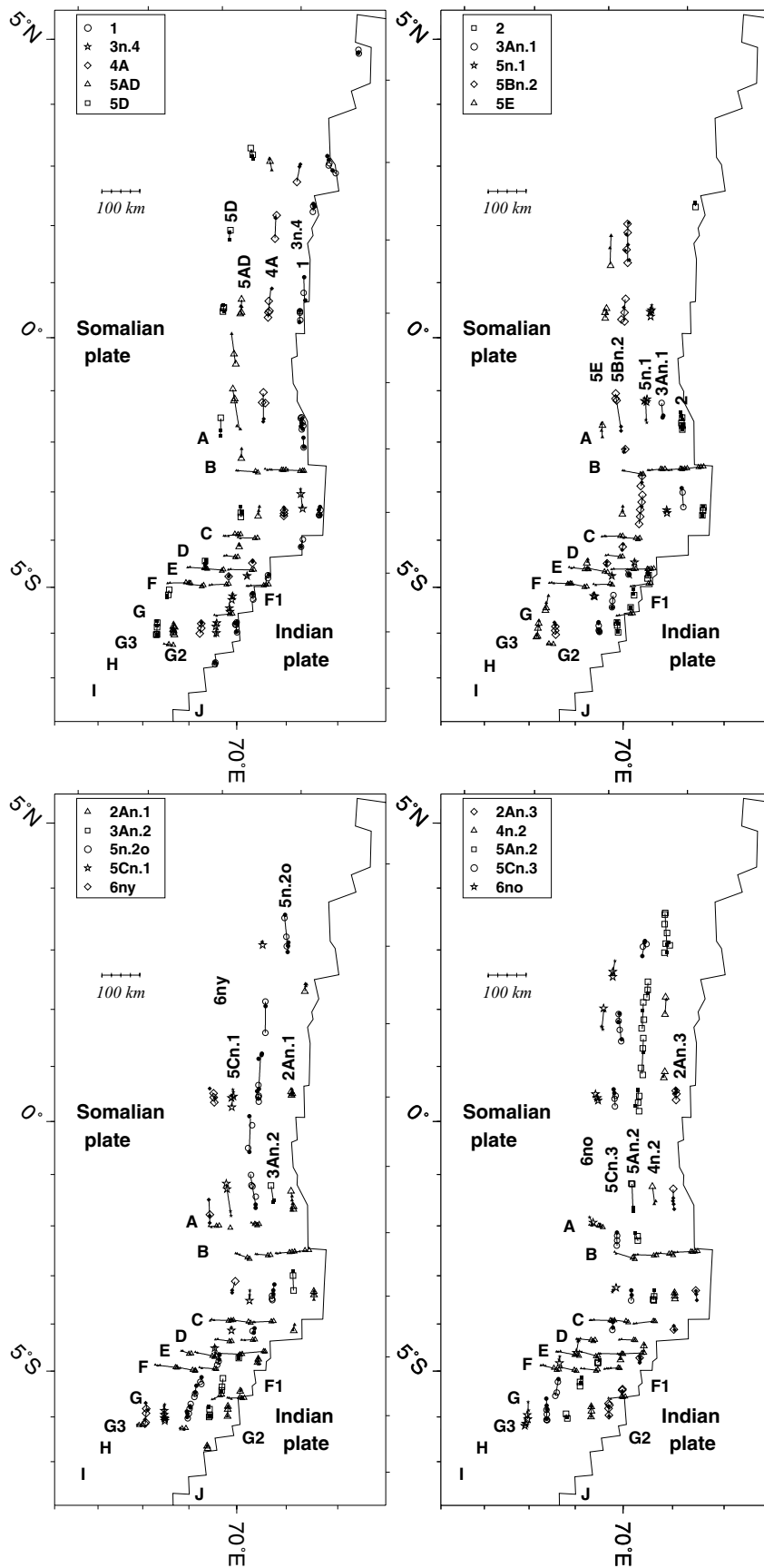
Figure 12. Anomaly and fracture zone crossings from the Indian Plate rotated onto the Somalian Plate using best-fitting rotations (Table 3). Solid and open symbols respectively show fixed and rotated data. Fracture zone crossings are shown with small triangles and align horizontally in the figure. Heavy lines show the present Carlsberg ridge. All panels are oblique Mercator projections about the mean India–Somalia pole of rotation since 20 Ma.

Table 3. Capricorn–Somalia and India–Somalia total rotations and covariances.

Chron	$\hat{\kappa}$	DOF†	Lat. °N	Long. °E	Ω (degrees)	Covariances a	b	c	d	e	f
Capricorn–Somalia											
1	1.08	181	11.66	51.22	−.537	103.4	119.7	−86.5	222.0	−110.6	76.5
2	1.12	125	10.92	49.18	−1.236	234.1	197.0	−176.1	315.2	−165.3	139.2
2An.1	.96	109	11.28	48.71	−1.685	127.6	159.2	−97.3	285.4	−128.3	78.7
2An.3	1.03	78	13.71	49.62	−2.238	193.7	173.3	−154.8	302.0	−140.4	127.9
3n.4	1.09	70	10.49	49.04	−3.322	280.2	342.0	−222.6	626.2	−275.1	187.0
3An.1	1.03	53	12.64	48.82	−3.687	493.1	596.8	−393.1	946.2	−491.2	325.3
3An.2	1.07	49	11.98	49.11	−4.203	816.4	964.8	−672.5	1309.0	−805.4	562.5
4n.2	1.05	52	11.62	49.74	−4.977	384.9	370.3	−347.4	518.0	−337.2	320.9
4A	1.10	52	13.95	48.20	−5.192	642.6	879.8	−503.6	1543.0	−707.7	411.1
5n.1	1.20	33	12.33	47.70	−5.777	1764.6	2912.1	−1202.7	5369.4	−1968.5	843.9
5n.2o	1.37	105	13.99	46.84	−6.258	751.9	953.8	−564.5	2098.3	−726.5	447.2
5An.2	1.42	50	14.23	45.81	−6.979	563.6	795.8	−407.7	2175.2	−556.1	322.2
5AD	1.91	46	16.06	44.47	−7.723	1330.6	2726.9	−917.1	6461.0	−1832.7	683.9
5Bn.2	1.76	28	16.73	43.98	−8.007	1771.5	3553.5	−1277.4	8607.0	−2449.7	1003.4
5Cn.1	1.29	38	15.14	44.92	−8.926	589.2	1010.3	−425.2	2256.6	−693.7	335.5
5Cn.3	1.01	42	15.66	44.48	−9.331	371.4	721.0	−253.7	1784.3	−475.8	195.2
5D	.95	39	16.24	43.92	−9.623	637.8	1405.4	−397.7	3504.8	−846.9	278.2
5E	1.16	40	16.08	44.33	−10.190	702.3	1348.3	−462.5	3159.4	−855.8	334.8
6ny	1.28	35	17.38	43.33	−10.309	1430.2	2436.0	−970.3	5314.8	−1611.2	703.1
6no	1.05	32	17.29	43.25	−10.895	514.8	1099.5	−347.0	2936.6	−710.1	256.2
India–Somalia											
1	1.13	32	24.86	25.17	−.304	458.3	594.3	−186.0	1135.0	−37.5	211.2
2	1.51	24	22.68	31.47	−.790	480.9	943.4	−74.5	2128.0	−11.8	85.1
2An.1	.92	28	21.40	34.37	−1.165	487.0	874.9	−84.6	1900.9	−14.2	85.2
2An.3	1.13	25	22.83	34.73	−1.602	602.7	1011.8	−191.8	2280.4	−.5	259.6
3n.4	1.11	14	21.85	33.62	−2.195	2392.1	5384.3	−150.0	12672.5	−99.0	135.1
3An.1	1.17	16	27.01	25.67	−2.174	2197.7	5380.9	74.8	13297.7	239.5	67.1
3An.2	1.66	13	27.46	25.56	−2.416	2445.7	5325.7	−210.4	11876.5	−362.9	65.6
4n.2	1.33	19	24.58	29.37	−3.024	585.1	1139.9	−72.4	2867.2	178.9	198.5
4A	1.49	23	22.96	32.12	−3.636	1933.3	3271.2	−318.7	6788.1	−20.5	326.2
5n.1	1.47	16	24.25	30.30	−3.792	4052.0	8393.9	52.5	19047.1	824.1	402.4
5n.2o	1.11	49	23.98	29.71	−4.337	579.7	1037.7	−25.6	2121.0	56.2	73.3
5An.2	1.35	36	23.62	30.63	−5.008	1084.7	1726.9	−60.2	4252.5	976.6	877.0
5AD	1.25	27	24.45	29.24	−5.665	893.4	1621.6	−121.3	3607.3	118.4	259.0
5Bn.2	1.37	35	23.32	31.75	−6.321	1151.3	2180.4	25.3	4678.2	306.8	174.7
5Cn.1	1.00	26	24.09	30.27	−6.529	750.9	1576.3	−85.9	4245.2	314.7	307.4
5Cn.3	1.12	28	23.60	31.75	−7.122	623.8	678.5	−332.4	1499.5	102.2	500.8
5D	1.48	25	25.32	30.50	−7.215	740.1	1200.1	−217.4	2455.9	−97.2	226.1
5E	1.22	23	24.90	30.96	−7.690	840.3	1274.9	−248.5	2804.7	1.7	265.3
6ny	2.22	22	24.62	31.13	−8.151	4358.2	9567.3	7.8	22071.8	331.9	313.5
6no	1.67	31	24.52	31.20	−8.589	1785.5	3582.8	197.8	7726.6	663.1	338.0

DOF† is degrees of freedom. See Table 2 for further details.

Rotations reconstruct the first plate relative to the second. Covariances are Cartesian and have units of 10^{-8} rad^2. Elements *a*, *d* and *f* are the variances of the (0°N, 0°E), (0°N, 90°E) and 90°N components of the rotation.

The covariance matrices are reconstructed as follows:

$$\begin{pmatrix} a & b & c \\ b & d & e \\ c & e & f \end{pmatrix}.$$

(Fig. 15). These 15 poles are located in the aseismic portion of the plate boundary between the western extensional zone and the eastern contractional zone, consistent with prior results (Gordon *et al.* 1990; Royer & Chang 1991; DeMets *et al.* 1994; Royer *et al.* 1997; Gordon *et al.* 1998).

Does India–Capricorn motion differ significantly from zero for the time interval from 20.1 to 7.9 Ma (Gordon *et al.* 1998)? Comparison of a null rotation to the 20.1–7.9 Ma stage rotation using the quadratic form of the chi-square test $\chi^2 = \mathbf{\Omega}^T \mathbf{C}_\Omega^{-1} \mathbf{\Omega}$, where $\mathbf{\Omega}$ is the (3x1) vector representation of the rotation (in the small angle approximation) and $\mathbf{C}_\Omega$ is the (3 × 3) covariance matrix, gives

$\chi^2 = 62.3$ ($p = 2 \times 10^{-13}$). Motion during this interval was thus significant.

The evolution of the India–Capricorn rotation angle over the past 20 Myr indicates a change in rate of rotation near 8 Ma. The open circles in the lower panel of Fig. 15 show the angles of rotation determined by differencing the best-fitting (i.e. unconstrained) India–Somalia and Somalia–Capricorn rotations. The size of these angles reflects not only the gradual increase with time of India–Capricorn motion, but also the change from reconstruction to reconstruction in the estimated position of the total pole of rotation. To obtain a set of angles that more consistently measure the progress of the
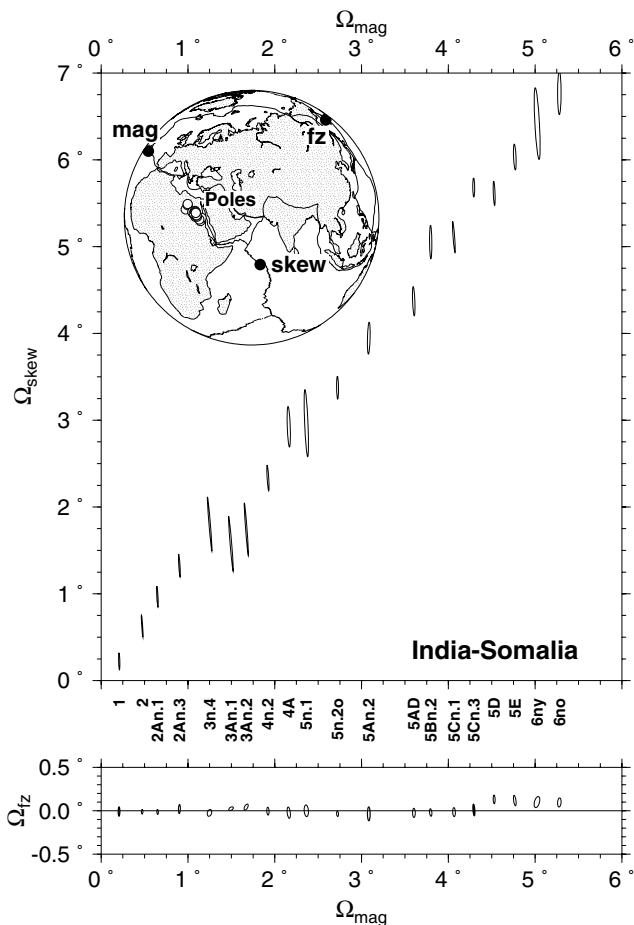
Figure 13. Orthogonal component plot of India–Somalia total rotations and 2-D 1σ error ellipses. Open circles on the inset globe show pole locations from Fig. 7. Ω_{skew}, Ω_{mag} and Ω_{fz} respectively are the components of rotation along the approximate locations of the skew misfit, magnetic anomaly misfit and fracture zone misfit eigenvectors, the locations of which are shown on the inset globe. The least uncertain component of rotation for the reconstructions is Ω_{mag}; its 1-D 1σ uncertainty averages $0.006°$, corresponding to an average 1σ displacement uncertainty of 0.6 km. The most uncertain component of rotation is Ω_{skew}; its 1-D 1σ uncertainty averages $0.10°$, corresponding to a 1σ displacement uncertainty as large as 1.6 km for points at the northwest end of the Carlsberg ridge, decreasing to zero for points close to this nearby partial uncertainty rotation. The intermediate uncertainty is Ω_{fz}; its 1-D 1σ uncertainty averages $0.019°$, corresponding to an average 1σ displacement uncertainty of 2.1 km.

rotation with time, we estimated a second set of angles constrained to a single pole of India–Capricorn rotation (the Fisher mean of all the estimated poles of total rotation each weighted by its angle of rotation, 4.3°S, 74.3°E). For each point in time, we then iteratively solved for the India–Capricorn rotation angle that gave the best least-squares fit to the corresponding anomaly and fracture zone crossings. This second set of angles is shown by filled triangles and is less dispersed than the first set of angles (lower panel in Fig. 15). Both sets of angles indicate a rate change near 8 Ma.

Fitting the 1040 India–Somalia data and the 1985 Capricorn–Somalia data for chrons 1no to 6no resulted in $\chi^2 = 1565.6$ for the set of rotations assuming a fixed India–Capricorn pole of rotation, which can be compared with the value of χ^2 of 1514.3 for the set of best-fitting (i.e. unconstrained) rotations. The difference, $\Delta\chi^2 = 51.3$, is insignificant ($p = 0.07$), indicating that the data
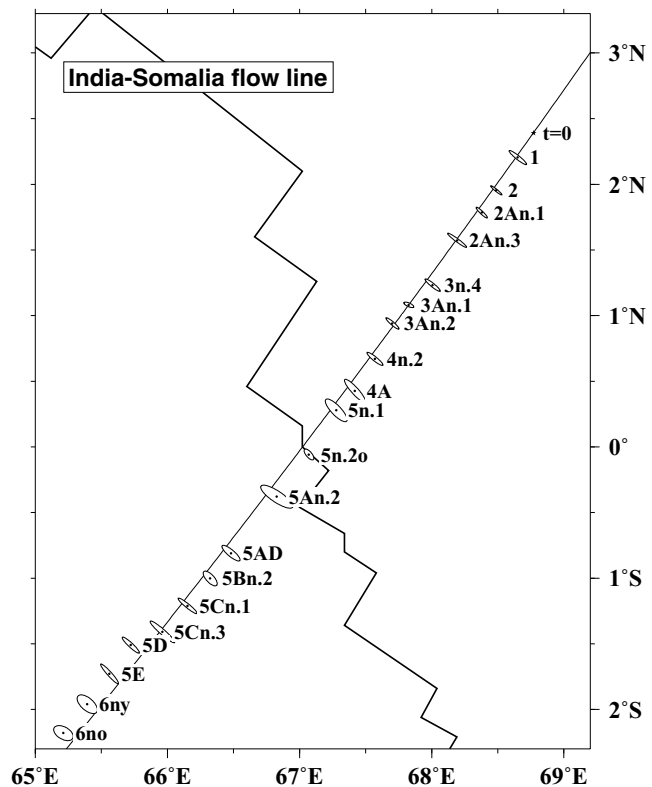

Figure 14. Displacement path of a point on the Indian Plate reconstructed relative to the Somalian Plate since C6no. The path originates at the old edge of anomaly 6 (solid star) on the Indian Plate and intersects the present boundary near its geographic centre. India–Somalia rotations and covariances (Table 3) are used to construct the path and 2-D 95 per cent confidence regions for rotated points. The dotted small circle is the one that best fits the reconstructed locations for C6no to the present.

are not inconsistent with a fixed pole of rotation during the entire 20 Myr interval. It may seem surprising that there can be a large and obvious change in stage pole location for Capricorn–Somalia rotation yet only an insignificant change in pole position for the India–Capricorn rotations derived from it. The explanation is that changes in Capricorn–Somalia pole position map mainly into changes not in India–Capricorn pole position but in India–Capricorn rotation rate. We solved for the best least-squares fit to the eight fixed-pole rotation angles for chrons 1no to 4n.2 using astronomically calibrated magnetic anomaly reversal ages and allowing for reversal age uncertainties of ±0.02 Myr (Fig. 15). The resulting best-fitting rotation rate and intercept are $0.28° \pm 0.01°$ Myr^{-1} (1σ) and $0.06° \pm 0.04°$ with χ^2 of 5.6 with 6 degrees of freedom, consistent with a steady rate of rotation over the past ≈8 Myr. When older chrons are included, linear regression of the time-series of best fixed-pole angles yields progressively larger misfits, with respective values of χ^2 of 11.6, 14.0 and 22.1 for chrons 4A, 5n.1 and 5n.2o, increasing to $\chi^2 = 186.8$ for chrons 1no to 6no. Linear regression of the fixed-pole angles for chrons 4A to 6no yields a best-fitting angular rotation rate of $0.11° \pm 0.01°$ Myr^{-1}, approximately 2.5 times slower than the angular rotation rate for chrons 1no to 4n.2. Thus, as is also evident in Fig. 15, the progression of angles with age is a much better fit if we divide the angles into two groups representing motion from the present to chron 4n.2 (7.9 Ma) and from chron 4A to chron 6no than if we fit them as if they correspond to a single angular velocity. The time-series of fixed pole angles for 20.1 to

Table 4. India–Capricorn total rotations and covariances.

Chron	Lat. °N	Long. °E	Ω (degrees)	Covariances					
				a	b	c	d	e	f
1	−3.55	74.85	.304	562.4	714.4	−272.5	1356.8	−147.7	287.1
2	−6.86	72.48	.569	717.8	1141.3	−250.1	2442.7	−176.1	221.9
2An.1	−7.91	73.06	.666	616.2	1034.9	−181.8	2185.9	−141.6	162.7
2An.3	−5.70	76.88	.843	800.3	1186.4	−345.9	2582.0	−139.3	384.1
3n.4	−7.91	72.13	1.427	2680.4	5729.9	−371.8	13296.9	−370.1	315.8
3An.1	−4.53	72.10	1.978	2713.2	5988.3	−317.3	14236.9	−239.6	376.9
3An.2	−5.19	71.49	2.323	3306.3	6310.5	−881.3	13172.4	−1143.1	597.0
4n.2	−4.90	73.07	2.501	996.2	1519.2	−419.7	3379.7	−146.6	498.9
4A	−3.50	75.96	2.052	2606.9	4169.0	−819.5	8322.8	−708.3	714.6
5n.1	−6.03	72.41	2.583	5891.1	11355.9	−1138.7	24391.8	−1086.1	1196.5
5n.2o	−4.15	74.88	2.578	1374.0	2011.7	−584.2	4208.8	−649.9	488.6
5An.2	−4.75	74.17	2.642	1678.0	2535.9	−464.0	6420.1	431.1	1177.1
5AD	−2.41	74.72	2.803	2299.1	4411.4	−1037.1	10033.2	−1660.5	902.9
5Bn.2	−2.76	76.99	2.351	3010.5	5805.1	−1246.9	13254.9	−2072.3	1120.8
5Cn.1	−3.85	74.28	3.240	1378.5	2610.9	−508.6	6488.7	−354.6	617.7
5Cn.3	−4.14	74.87	3.005	1015.2	1414.4	−584.6	3276.5	−359.5	683.3
5D	−4.67	73.27	3.289	1408.2	2631.5	−613.7	5946.5	−921.5	488.3
5E	−4.56	74.39	3.435	1582.6	2652.6	−705.9	5950.0	−823.3	574.1
6ny	−3.35	76.31	3.047	5872.5	12060.8	−947.3	27362.3	−1213.3	956.9
6no	−3.08	75.79	3.221	2331.2	4708.3	−147.0	10650.6	−24.4	575.8

Rotations reconstruct the Indian Plate relative to an arbitrarily fixed Capricorn Plate. The caption to Table 3 describes how the covariance matrices were determined.

7.9 Ma is generally consistent with steady India–Capricorn motion prior to 7.9 Ma, although we cannot rule out more complicated models in which intervals of faster motion separate intervals of slow or no motion. For example, it is possible that there was motion between ≈20 and ≈15 Ma with no motion between ≈15 and ≈8 Ma.

Although a change in the India–Capricorn stage pole of rotation is not formally statistically significant, several lines of evidence suggest such a change (Fig. 15). Poles of rotation for reconstructions for the past 8 Myr tend to lie to the south-southwest of poles of rotation for reconstructions for 11 to 20 Ma, consistent with a modest change in stage pole position near 8 Ma (Fig. 15). Such a change would also be consistent with the interpretation that India–Somalia rotation was steady for the past 20 Myr while Capricorn–Somalia rotation consists of two stages with the change in stage pole location occurring near 8 Ma, as discussed above.

The evolution of the stage pole of rotation is best examined in an orthogonal component plot (Fig. 16). The three eigenvectors approximately correspond to:

(i) the difference between the India–Somalia and Capricorn–Somalia magnetic anomaly misfit eigenvectors ($\Omega_{\Delta mag}$);

(ii) the difference between the India–Somalia and Capricorn–Somalia fracture zone misfit eigenvectors ($\Omega_{\Delta fz}$); and

(iii) the difference between the India–Somalia and Capricorn–Somalia skew misfit eigenvectors ($\Omega_{\Delta skew}$).

Because each India–Capricorn rotation is found by differencing two rotations with a large component in common, the component angles for each India–Capricorn rotation are smaller than found for the coeval India–Somalia or Capricorn–Somalia rotation. In particular, the India–Capricorn $\Omega_{\Delta mag}$ component is a factor of 10 to 16 times smaller than Ω_{mag} for India–Somalia motion or for India–Capricorn motion (Figs 8, 13 and 16). Moreover, the India–Capricorn rotation uncertainties are larger than for either the India–Somalia or Capricorn–Somalia rotations by roughly a factor of $\sqrt{2}$ (Fig. 16). Thus, the signal-to-noise ratio is lower for India–Capricorn rotations than for India–Somalia or Capricorn–Somalia rotations. In both the

plot of $\Omega_{\Delta fz}$ versus $\Omega_{\Delta mag}$ and the plot of $\Omega_{\Delta skew}$ versus $\Omega_{\Delta mag}$, a thin-dashed reference line connects the points corresponding to the most ancient (chron 6no) and most recent (chron 1no) reconstructions. In the plot of $\Omega_{\Delta fz}$ versus $\Omega_{\Delta mag}$, the data tend to lie below the reference line and, in the plot of $\Omega_{\Delta skew}$ versus $\Omega_{\Delta mag}$, the data tend to lie above the reference line. Thus, both plots suggest that at least one change in stage pole occurred during the past 20 Myr. A thick grey line segment in each plot connects the most ancient reconstruction (chron 6no) to that for ≈8 Ma (chron 4n.2) and a second segment connects the latter point to the most recent reconstruction (chron 1no), following the timing suggested by the change in rate of rotation (Fig. 15) and the change in Capricorn–Somalia pole location (Fig. 8).

The reconstructed displacement paths of three points located near the northern edge of the Capricorn Plate (Fig. 15) are shown in the upper and middle rows of panels in Fig. 17. The upper row shows the unconstrained estimates of rotation while the middle row shows estimates constrained to a two-stage rotation corresponding to the grey lines in Fig. 16. For both unconstrained and two-stage estimates, the displacements for points B and C since ≈8 Ma are faster and in a more northerly direction than before ≈8 Ma (Fig. 17).

4.5 Comparison to marine seismic estimates of convergence

Estimates of north–south convergence since 8 Ma across the equatorial deforming zone are available from three north–south marine seismic profiles that image thrust faults in the contractional part of the India–Capricorn plate boundary. Profiles located along 78.8°E and 81.5°E (Chamot-Rooke *et al.* 1993; Van Orman *et al.* 1995) span the entire deforming zone and a third, at 84.5°E (Jestin 1994), crosses only part of the plate boundary and thus gives only a lower bound for the total convergence.

The amount of north–south convergence indicated by the 7.9 Ma (chron 4n.2) rotation significantly exceeds the convergence estimated for all three profiles (Fig. 18). There are several possible
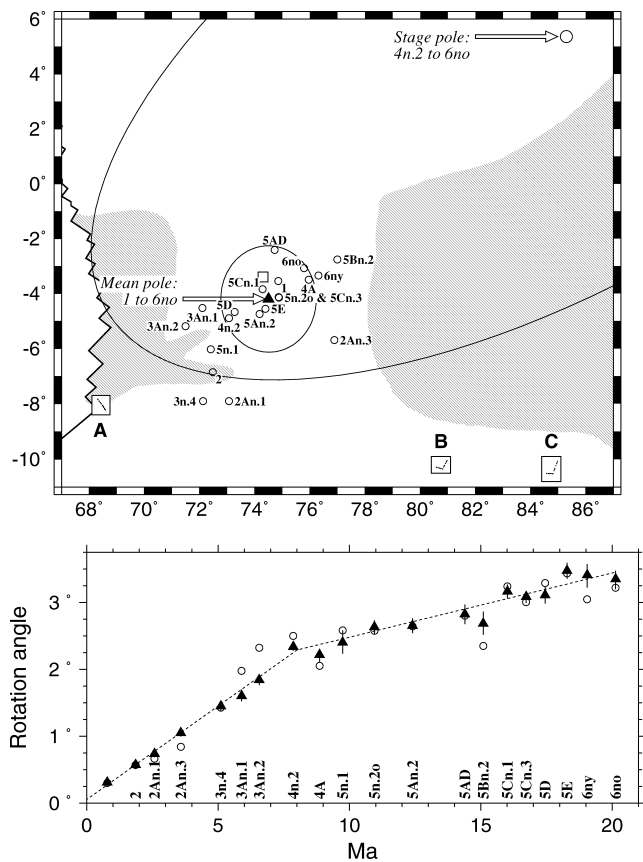
Figure 15. Upper: India–Capricorn poles of rotation (Table 4). The tiny open circles show the poles of rotations found by differencing coeval best-fitting India–Somalia and Capricorn–Somalia rotations for the 20 points in time investigated in this paper. The filled triangle shows the Fisher mean of these 20 poles. The open square shows the pole of rotation for the 3-Myr-average angular velocity estimated by DeMets *et al.* (1994). Subregions A, B and C show displacement paths of three points on the Capricorn Plate relative to an arbitrarily fixed Indian Plate; these plots are shown enlarged in Fig. 17. Lower: India–Capricorn rotation angles versus age. The angles are shown by circles if for unconstrained poles of rotation and shown by triangles if the India–Capricorn rotation is constrained to be about the Fisher mean pole.

explanations including significant displacement out of the plane of the seismic profile or significant faulting with offset less than the threshold of detection of the seismic profiles. Along all three profiles, the reconstructions suggest that a small component of north–south extension and not north–south shortening occurred from 20.1 to 7.9 Ma. Thus, our results suggest that the widespread unconformity in the Bengal fan dated at 7.5 to 8 Ma records the onset of contractional deformation, although motion between the India and Capricorn plates clearly began long before 8 Ma. It is interesting that the estimates of convergence from the seismic profiles agree better with the net convergence since 20.1 Ma than with the convergence since 7.9 Ma, suggesting that many of the faults that have accommodated shortening during the past ≈8 Myr may have accommodated substantial extension before ≈8 Ma.

5 CONCLUSIONS

(i) The results show that the episode of India–Capricorn motion with contraction in the Central Indian basin began approximately 8 Ma, consistent with the timing of the onset of thrust faulting in-
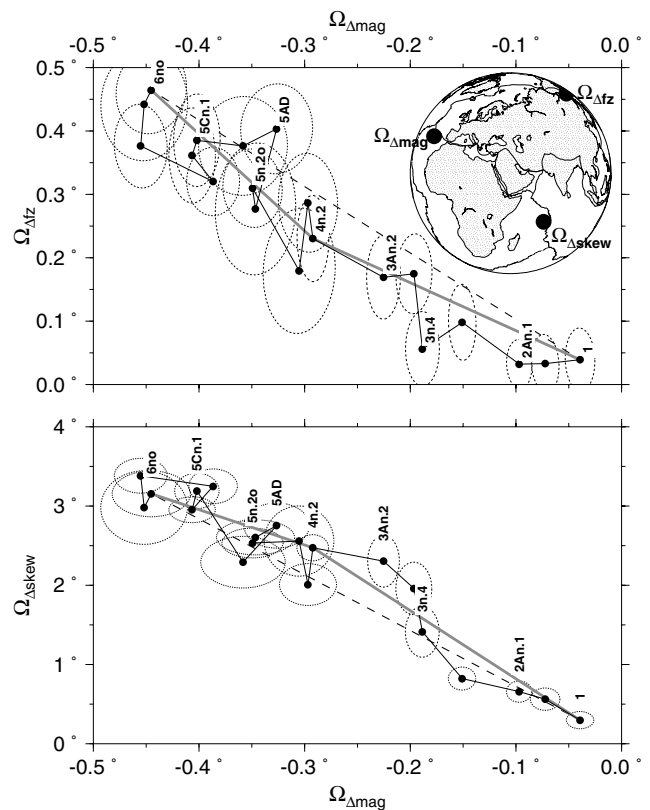

Figure 16. Orthogonal component plot of India–Capricorn total rotations and 2-D 1σ error ellipses. $\Omega_{\Delta skew}$, $\Omega_{\Delta mag}$ and $\Omega_{\Delta fz}$ respectively are the components of rotation along the approximate locations of the three eigenvectors, corresponding to the respective differences between the India–Somalia and Capricorn–Somalia skew misfit, the India–Somalia and Capricorn–Somalia magnetic anomaly misfit, and the India–Somalia and Capricorn–Somalia fracture zone misfit eigenvectors. The locations of these (approximate) eigenvectors are shown on the inset globe. The least uncertain component of rotation for the reconstructions is $\Omega_{\Delta mag}$; its 1-D 1σ uncertainty averages 0.017°, corresponding to an average 1σ displacement uncertainty of 1.9 km at reference point A (Figs 15 and 17). The most uncertain component of rotation is $\Omega_{\Delta skew}$; its 1-D 1σ uncertainty averages 0.176°, corresponding to an average 1σ displacement uncertainty of 1.3 km for this nearby pole of rotation. The intermediate uncertainty is $\Omega_{\Delta fz}$; its 1-D 1σ uncertainty averages 0.048°, corresponding to an average 1σ displacement uncertainty of 5.3 km. Grey straight line segments show an interpretation of these rotations in terms of two successive fixed stage poles of rotation with the change in stage pole occurring at chron 4n.2 (7.9 Ma).

dicated by seismic stratigraphy and deep sea drilling (Moore *et al.* 1974; Weissel *et al.* 1980; Curray & Munasinghe 1989; Cochran *et al.* 1990). The observed motion between India and Capricorn plates since 8 Ma appears steady with little indication of episodic motion. Minor increases and decreases in spreading rate on a fine timescale during that interval cannot be excluded, but major increases and decreases in rate on a timescale of millions of years can be excluded.

(ii) The reconstructions indicate that additional India–Capricorn motion occurred between 8 and 20 Ma (Gordon *et al.* 1998), which is in conflict with many interpretations of the seismic stratigraphy and deep sea drilling (Moore *et al.* 1974; Weissel *et al.* 1980; Curray & Munasinghe 1989; Cochran *et al.* 1990). From ≈20 to ≈8 Ma, the displacement accommodated across the Central Indian basin was mainly eastward motion of the Capricorn Plate relative to the Indian
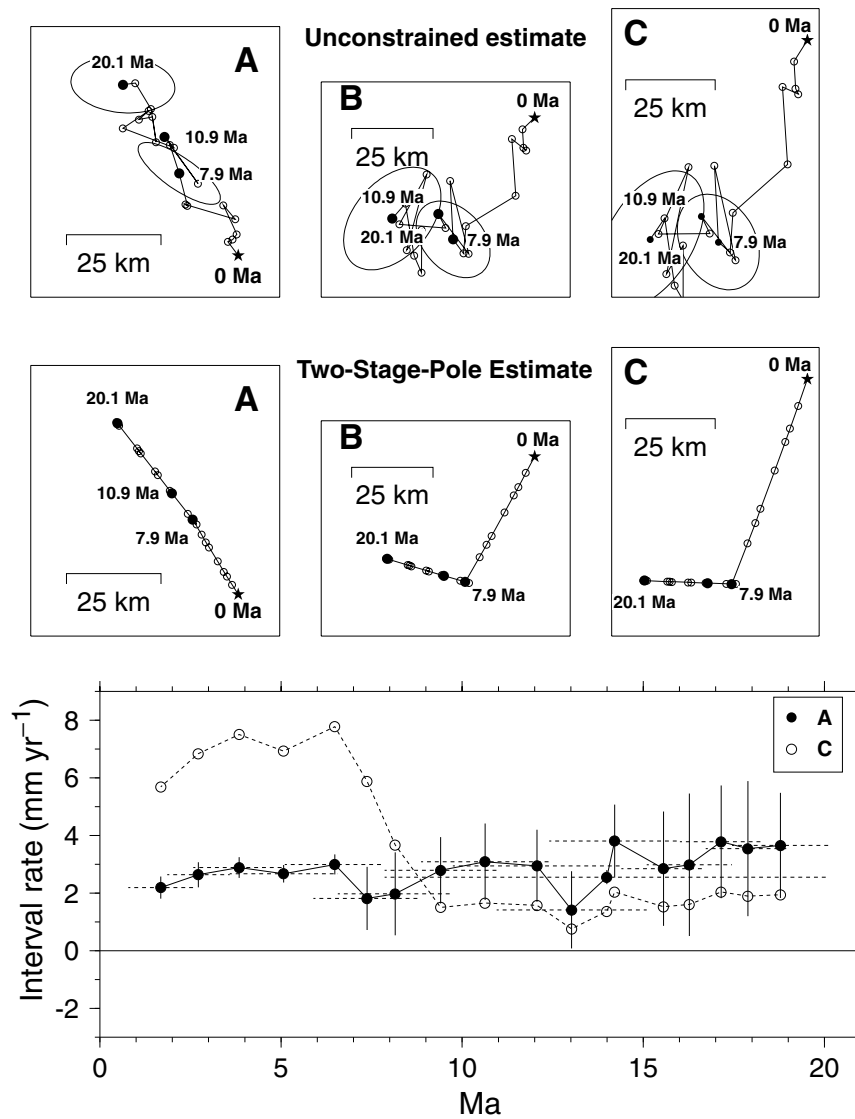
Figure 17. The upper and middle panels show displacement paths for points A, B and C near the assumed northern edge of the Capricorn Plate relative to an arbitrarily fixed Indian Plate (Fig. 15). The present position of each point is shown by a star. Reconstructed points are shown by circles, which are filled for 7.9 Ma (chron 4n.2), 10.9 Ma (chron 5no.2) and 20.1 Ma (chron 6no), and open otherwise. Ninety-five per cent confidence regions are shown for 7.9 and 20.1 Ma. The upper panels are constructed using the unconstrained estimates of India–Capricorn motion found by differencing coeval best-fitting India–Somalia and Capricorn–Somalia rotations (Table 4). The middle panels are constructed by finding the best-fitting India–Capricorn angle of rotation while the pole of rotation is constrained to consistency with a two-stage-pole model. From the present to chron 4n.2, the India–Capricorn pole of rotation is constrained to be the Fisher mean of the e poles for chrons 1no to 4n.2; from chron 4n.2 to chron 6no the additional rotation beyond that for chron 4n.2 is constrained to be about the stage pole determined by differencing the chron 6no finite rotation and the mean chron 4n.2 rotation used in this estimate. The lowest panel shows India–Capricorn interval rates (circles) along displacement paths A and C estimated from the middle panels (i.e. two-stage-pole rotation estimates). Rate uncertainties for path C, which average ± 2–3 mm yr^{-1}, are omitted. Reversal ages are from Cande & Kent (1995). Dotted horizontal lines indicate the interval used for estimating a given rate. Uncertainties in all panels are 1σ.

Plate before changing to faster nearly northward motion near 8 Ma. This earlier motion was at a slower rate than the post-8 Ma motion. Motion before $\approx$8 Ma may have been steady. Alternatively, no motion may have occurred between approximately 15 and 8 Ma, with all the prior motion occurring between 15 and 20 Ma. Some other more complicated histories are also consistent with the data. Where and how this motion was accommodated is unclear.

(iii) Our most surprising result is the general absence of change in the India–Somalia pole location over the past 20 Myr. Given the change in forces and torque across the India–Capricorn boundary

we assume occurred at $\approx$8 Ma, it is surprising that the motion of India changed so little, if at all.

(iv) Over the past 12.4 Ma, over which the geomagnetic reversal timescale is astronomically calibrated, Capricorn–Somalia and India–Somalia seafloor spreading rates both exhibit small but significant changes in spreading rate. Capricorn–Somalia spreading slowed by $\approx$6 mm yr^{-1} at 11 to 10 Ma and India–Somalia spreading slowed by $\approx$5 mm yr^{-1} at 8 to 7 Ma. Both rates have increased slightly during the past 8 Myr. Estimates of India–Somalia seafloor spreading rates from continuous geodetic sites on these two plates
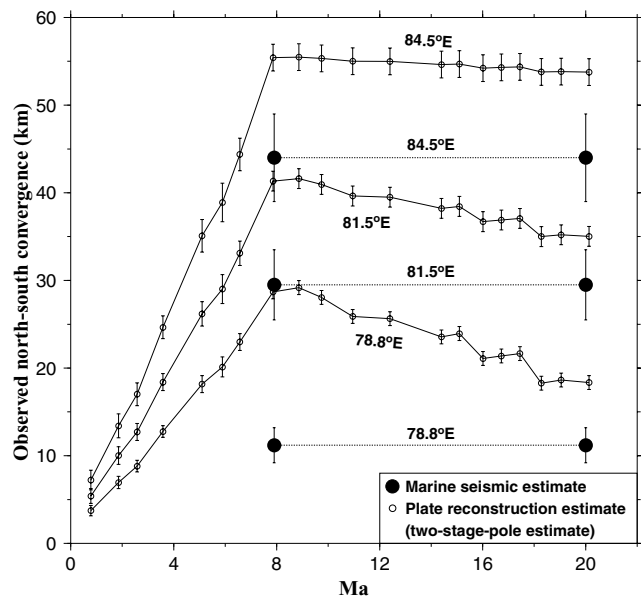
Figure 18. Comparison of the north–south component of convergence estimated from plate reconstructions (two-stage-pole estimates) and from throws on faults for north–south seismic profiles along 78.8°E, 81.5°E and 84.5°E (Chamot-Rooke *et al.* 1993; Jestin 1994; Van Orman *et al.* 1995). Solid circles show north–south convergence (with 1σ uncertainty) estimated from seismic profiles. Open circles show convergence (with 1σ uncertainty) estimated from the plate reconstructions.

should soon allow for a further test of the apparent increase in India–Somalia spreading rate.

(v) We attribute the change in Capricorn Plate motion at ≈8 Ma to a change in the forces acting on the edges of the Capricorn Plate (Gordon *et al.* 1978). Explanations of the cause of the change at ≈8 Ma in Capricorn Plate motion will require modelling of the torques acting on the collisional boundaries of the Indian and Capricorn plates and the mechanics of stress transfer across their shared boundary.

ACKNOWLEDGMENTS

REFERENCES

Abdul Aziz, H., Krijgsman, W., Hilgen, F.J., Wilson, D.S. & Calvo, J.P., 2003. An astronomical polarity timescale for the late middle Miocene based on cyclic continental sequences, *J. geophys. Res.,* **108,** doi: 10.1029/2002JB001818.

Atwater, T. & Mudie, J.D., 1973. Detailed near-bottom geophysical study of the Gorda Rise, *J. geophys. Res.,* **78,** 8665–8686.

Briais, A., 1995. Structural analysis of the segmentation of the Central Indian ridge between 20°30′S and 25°30′S (Rodriguez triple junction), *Mar. Geophys. Res.,* **17,** 431–467.

Cande, S.C. & Kent, D.V., 1992. A new geomagnetic polarity time scale for the Late Cretaceous and Cenozoic, *J. geophys. Res.,* **97,** 13 917–13 951.

Cande, S.C. & Kent, D.V., 1995. Revised calibration of the geomagnetic polarity timescale for the Late Cretaceous and Cenozoic, *J. geophys. Res.,* **100,** 6093–6095.

Chamot-Rooke, N., Jestin, F., de Voogd, B. & Phèdre Working Group, 1993. Intraplate shortening in the central Indian Ocean determined from a 2100-km-long north–south deep seismic reflection profile, *Geology,* **21,** 1043–1046.

Chang, T., 1988. Estimating the relative rotation of two tectonic plates from boundary crossings, *J. Am. Stat. Assoc.,* **83,** 1178–1183.

Chang, T., Stock, J. & Molnar, P., 1990. The rotation group in plate tectonics and the representation of uncertainties of plate reconstructions, *Geophys. J. Int.,* **101,** 649–661.

Chaubey, A.K., Krishna, K.S., Subba Raju, L.V. & Gopala Rao, D., 1990. Magnetic anomalies across the southern Central Indian Ridge: evidence for a new transform fault, *Deep-Sea Res.,* **37,** 647–656.

Chaubey, A.K., Bhattacharya, G.C., Murty, G.P.S. & Desa, M., 1993. Spreading history of the Arabian Sea: Some new constraints, *Mar. Geol.,* **112,** 343–352.

Cochran, J.R. *et al.*, 1990. Himalayan uplift, sea level, and the record of Bengal Fan sedimentation at the ODP leg 116 sites, *Proc. ODP, Sci. Results,* **116,** 397–414, Ocean Drilling Program, College Station, Texas.

Curray, J.R. & Munasinghe, T., 1989. Timing of intraplate deformation, northeastern Indian Ocean, *Earth planet. Sci. Lett.,* **94,** 71–77.

DeMets, C., Gordon, R.G., & Vogt, P., 1994. Location of the Africa-Australia-India triple junction and motion between the Australian and Indian plates: Results from an aeromagnetic investigation of the Central Indian and Carlsberg ridges, *Geophys. J. Int.,* **119,** 893–930.

Dyment, J., 1991. Structure et évolution de la lithosphère océanique dans l'océan Indien: Apport des anomalies magnétiques, *PhD thesis*, Université de Strasbourg, Strasbourg.

Eittreim, S. & Ewing, J., 1972. Mid-plate tectonics in the Indian Ocean, *J. geophys. Res.,* **77,** 6413–6421.

Fisher, R.L., Sclater, J.G. & McKenzie, D.P., 1971. Evolution of the central Indian Ridge, western Indian Ocean, *Geol. Soc. Am. Bull.,* **82,** 553–562.

Glebovsky, V.Y. *et al.*, 1995. Mid-oceanic ridges and deep ocean basins: AMF structure, in *Anomalous magnetic field of the world ocean,* pp. 67–144, ed. Gorodnitsky, A.M., CRC Press, Boca Raton.

Gordon, R.G., 1998. The plate tectonic approximation: plate nonrigidity, diffuse plate boundaries, and global plate reconstructions, *Annu. Rev. Earth Pl. Sci.,* **26,** 615–642.

Gordon, R.G., 2000. Diffuse oceanic plate boundaries: Strain rates, vertically averaged rheology, and comparisons with narrow plate boundaries and stable plate interiors, *Am. geophys. Un. Monogr.,* **121,** 143–159.

Gordon, R.G., Harter, C.E. & Cox, A., 1978. Absolute motion of an individual plate from its ridge and trench boundaries, *Nature,* **274,** 752–755.

Gordon, R.G., DeMets, C. & Argus, D.F., 1990. Kinematic constraints on distributed lithospheric deformation in the equatorial Indian Ocean from present motion between the Australian and Indian plates, *Tectonics,* **9,** 409–422.

Gordon, R.G., DeMets, C. & Royer, J.Y., 1998. Evidence for long-term diffuse deformation of the lithosphere of the equatorial Indian Ocean, *Nature,* **395,** 370–374.

Harrison, T.M., Copeland, P., Kidd, W.S. F. & Yin, A., 1992. Raising Tibet, *Science,* **255,** 1663–1670.

Hellinger, S.J., 1979. The statistics of finite rotations in plate tectonics, *PhD thesis*, Massachusetts Institute of Technology, Cambridge, p. 172, unpublished work.

Hilgen, F.J., Krijgsman, W., Langereis, C.G., Lourens, L.J., Santarelli, A. & Zachariasse, W.J., 1995. Extending the astronomical (polarity) time scale into the Miocene, *Earth planet. Sci. Lett.,* **136,** 495–510.

Jestin, F., 1994. Cinématique rigide et déformations dans la jonction triple Afar et dans le basin Indien Central, *PhD thesis*, Université Pierre et Marie Curie, Paris.

Karasik, A.M., Mercuriev, S.A., Mitin, L.I., Sochevanova, N.A. & Yanovsky, V.N., 1986. Peculiarities in the history of opening of the Arabian Sea from systematic magnetic survey data, *Documents of the Academy of Sciences of USSR,* **286,** 933–938.

Klitgord, K.D., Heustis, S.P., Mudie, J.D. & Parker, R.L., 1975. An analysis of near-bottom magnetic anomalies: seafloor spreading and the magnetized layer, *Geophys. J. R. astr. Soc.,* **43,** 387–424.

Krijgsman, W., Hilgen, F.J., Raffi, I., Sierro, F.J. & Wilson, D.S., 1999. Chronology, causes, and progression of the Messinian salinity crisis, *Nature,* **400,** 652–655.

Krishna, K.S., Bull, J.M. & Scrutton, R.A., 2001. Evidence for multi-phase folding of the central Indian Ocean lithosphere, *Geology,* **29,** 715–718.

Molnar, P. & Stock, J.M., 1985. A method for bounding uncertainties in combined plate reconstructions, *J. geophys. Res.,* **90,** 12 537–12 544.

Molnar, P., Pardo-Casas, F. & Stock, J., 1988. The Cenozoic and Late Cretaceous evolution of the Indian Ocean Basin: Uncertainties in the reconstructed positions of the Indian, African and Antarctic plates, *Basin Res.,* **1,** 23–40.

Molnar, P., England, P. & Martinod, J., 1993. Mantle dynamics, uplift of the Tibetan plateau, and the Indian monsoon, *Rev. Geophys.,* **31,** 357–396.

Moore, D.G., Curray, J.R., Raitt, R.W. & Emmel, F.J., 1974. Stratigraphic-seismic section correlations and implications to Bengal Fan history, *Initial Rep. Deep Sea,* **22,** 403–412.

Müller, R.D., Sandwell, D.T., Tucholke, B.E., Sclater, J.G. & Shaw, P.R., 1991. Depth to basement and geoid expression of the Kane fracture zone: A comparison, *Mar. Geophys. Res.,* **13,** 105–129.

Parson, L.M., Patriat, P., Searle, R.C. & Briais, A.R., 1993. Segmentation of the Central Indian Ridge between 12°12′S and the Indian Ocean triple junction, *Mar. Geophys. Res.,* **15,** 265–282.

Patriat, P., 1987. *Reconstitution de l'évolution du système de dorsales de l'océan Indien par les méthodes de la cinématique des plaques,* Publ. Territoire des Terres Australes et Antarctiques Francaises, Paris.

Ramana, M.V., Ramprasad, T., Kamesh Raju, K.A. & Desa, M., 1993. Geophysical studies of the Carlsberg ridge, Indian Ocean, *Mar. Geol.,* **115,** 21–28.

Royer, J.-Y. & Chang, T., 1991. Evidence for relative motions between the Indian and Australian plates during the last 20 Myr from plate tectonic reconstructions: Implications for the deformation of the Indo-Australian plate, *J. geophys. Res.,* **96,** 11 779–11 802.

Royer, J.-Y. & Gordon, R.G., 1997. The motion and boundary between the Capricorn and Australian plates, *Science,* **277,** 1268–1274.

Royer, J.-Y., Gordon, R.G., DeMets, C. & Vogt, P.R., 1997. New limits on the motion between India and Australia since chron 5 (11 Ma) and implications for lithospheric deformation in the equatorial Indian Ocean, *Geophys. J. Int.,* **129,** 41–74.

Sandwell, D.T., 1984. A detailed view of the south Pacific geoid from satellite altimetry, *J. geophys. Res.,* **89,** 1089–1104.

Sandwell, D.T. & Smith, W.H.F., 1997. Marine gravity anomaly from Geosat and ERS 1 satellite altimetry, *J. geophys. Res.,* **102,** 10 039–10 054.

Schouten, H. & McCamy, K., 1972. Filtering marine magnetic anomalies, *J. geophys. Res.,* **77,** 7089–7099.

Tisseau, J., 1978. Etude structurale du Golfe d'Aden et du bassin de Somalie (Océan Indien occidental nord), *Thèse de 3ème cycle,* Université Paris-Sud, Paris.

Van Orman, J., Cochran, J.R., Weissel, J.K. & Jestin, F., 1995. Distribution of shortening between the Indian and Australian plates in the central Indian Ocean, *Earth planet. Sci. Lett.,* **133,** 35–46.

Weissel, J.K., Anderson, R.N. & Geller, C.A., 1980. Deformation of the Indo-Australian plate, *Nature,* **287,** 284–291.

Wessel, P. & Smith, W.H.F., 1991. Free software helps map and display data, *EOS, Trans. Am. geophys. Un.,* **72,** 441–446.

Wiens, D.A. *et al.*, 1985. A diffuse plate boundary model for Indian Ocean tectonics, *Geophys. Res. Lett.,* **12,** 429–432.

Wilson, D.S., 1993a. Confidence intervals for motion and deformation of the Juan de Fuca plate, *J. geophys. Res.,* **98,** 16 053–16 071.

Wilson, D.S., 1993b. Confirmation of the astronomical calibration of the magnetic polarity timescale from sea-floor spreading rates, *Nature,* **364,** 788–790.

Zijderveld, J.D., 1967. A.C. demagnetization of rocks: Analysis of results, in *Methods in Palaeomagnetism,* pp. 254–286, eds Collinson, D.W., Creer, K.M. & Runcorn, S.K., Elsevier, Amsterdam.
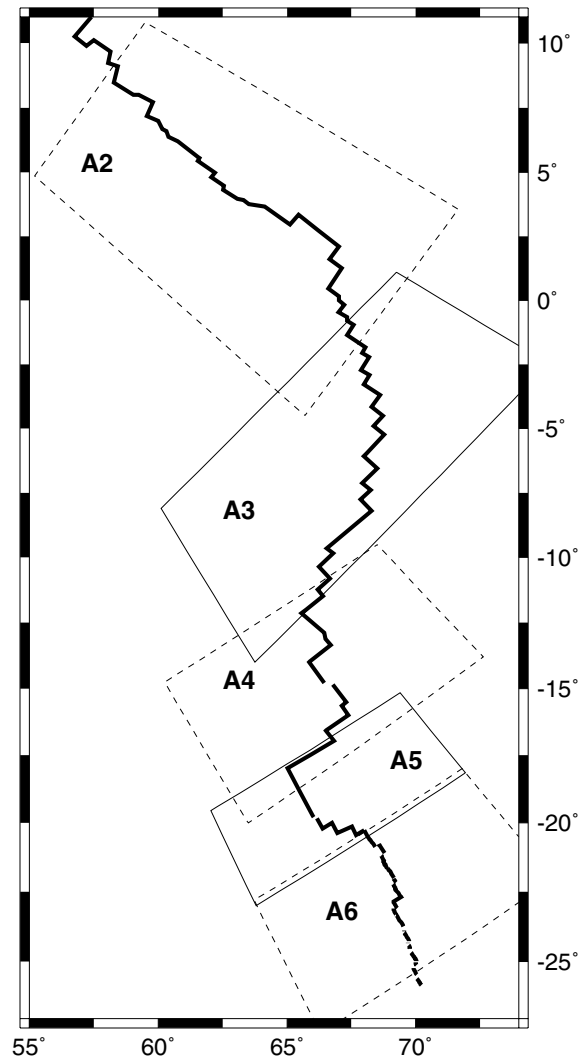
APPENDIX A
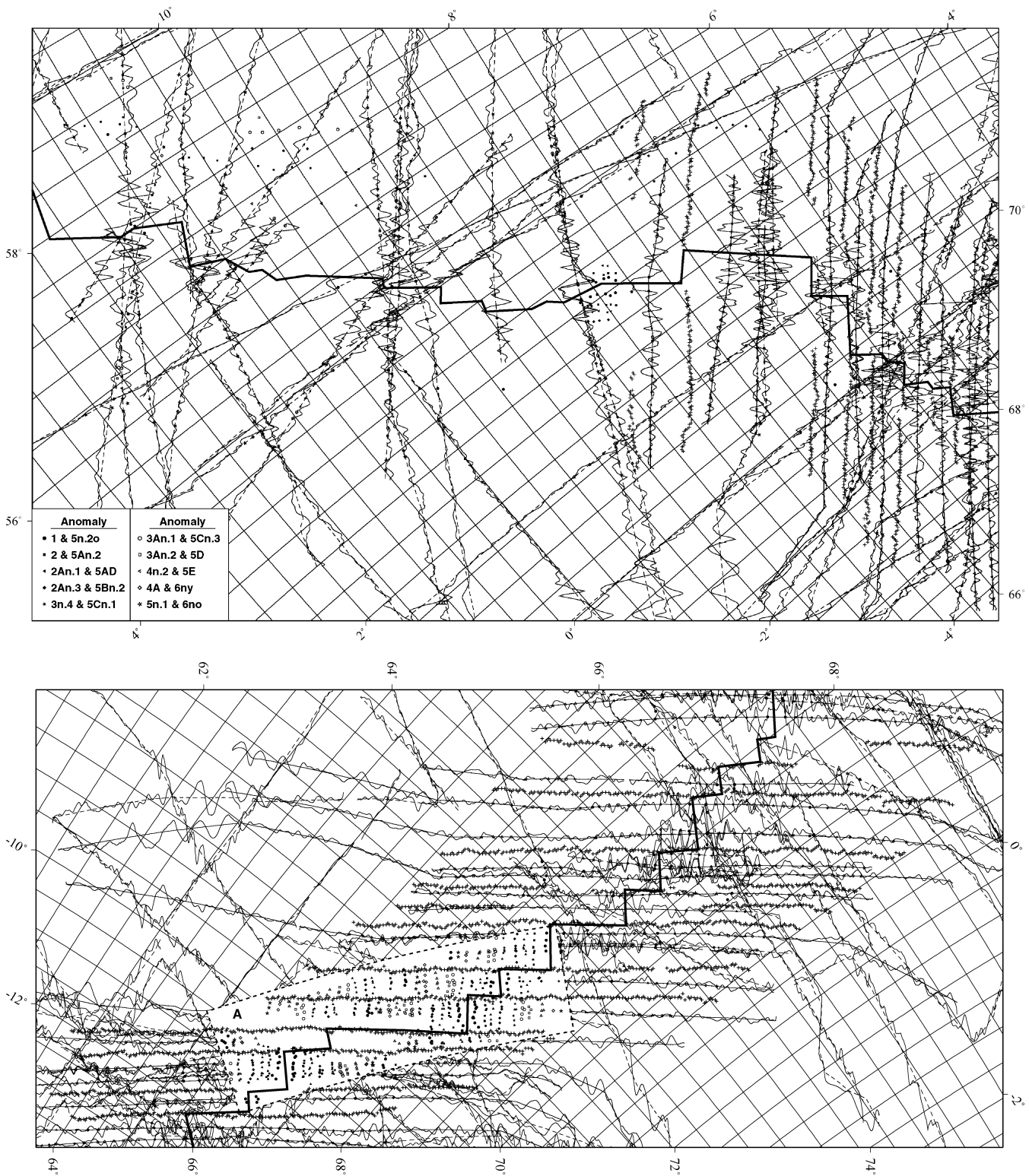

Figure A1: Location map for Figs A2–A6.

Figure A2–A6: Airborne and shipboard magnetic profiles across the Carlsberg and Central Indian ridges. Dashed lines show tracks for shipboard cruises or Project Magnet flights. Solid lines show tracks for flights during a 1990 aeromagnetic survey (DeMets *et al.* 1994). All magnetic profiles are reduced to the pole and are projected toward 45°NW for visual clarity. Legend in left corner of Fig. A2 shows the symbols used to denote different anomaly crossings. All anomaly crossings not associated with a ship or airplane track were digitized from analogue profiles or are from other sources (see text). Crosses mark the locations of gravity lows that follow fracture zone troughs. South of 20.5°S, the present plate boundary is adopted from Briais (1995); north of 20.5°S, the plate boundary is defined from magnetic profiles, marine gravity and GLORIA long-range side-scan sonar observations (Parson *et al.* 1993). Magnetic profiles from area C in Fig. 6 mainly sample anomaly 1 (i.e. the central anomaly) and are omitted as a result of their dense spacing.
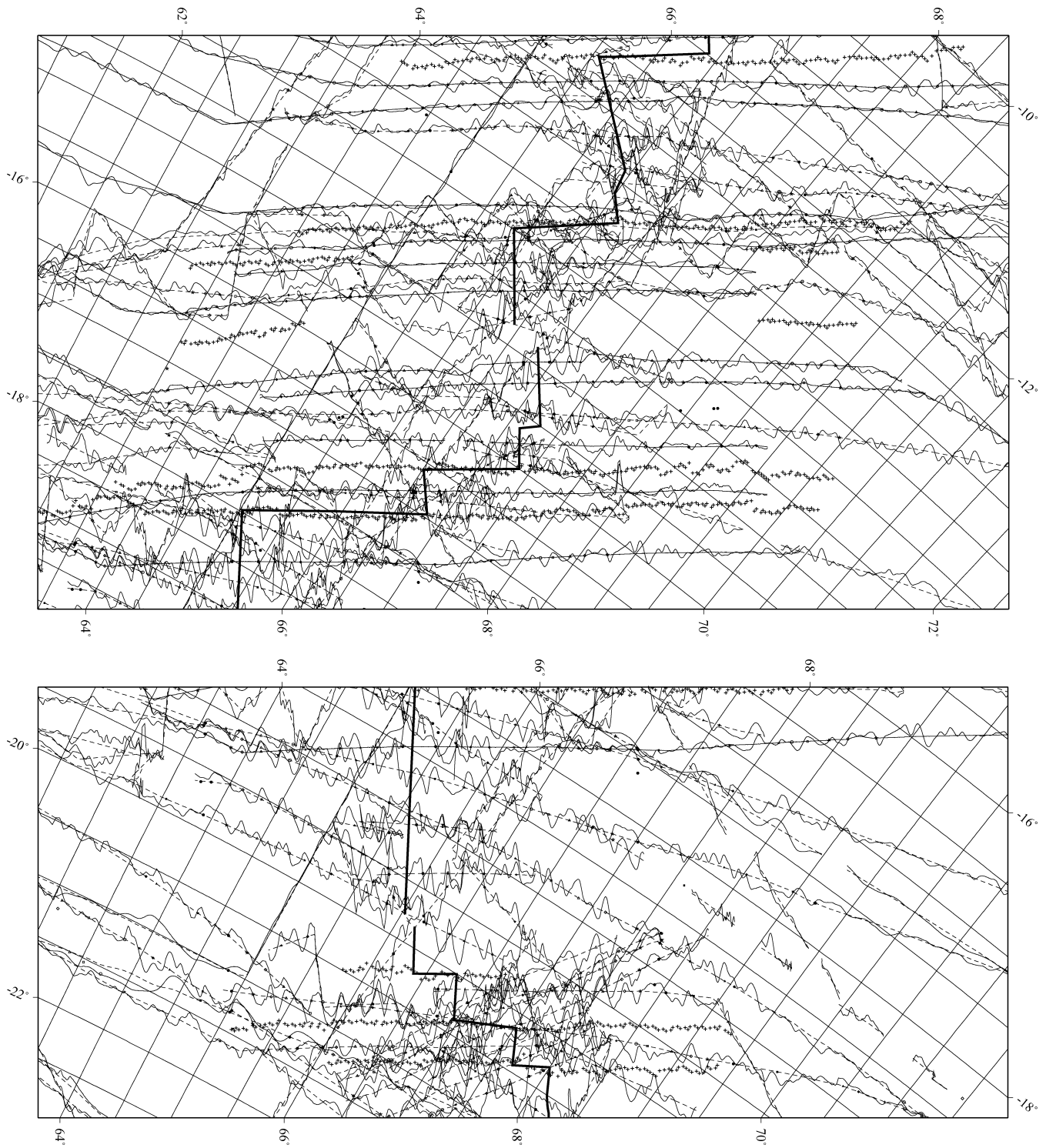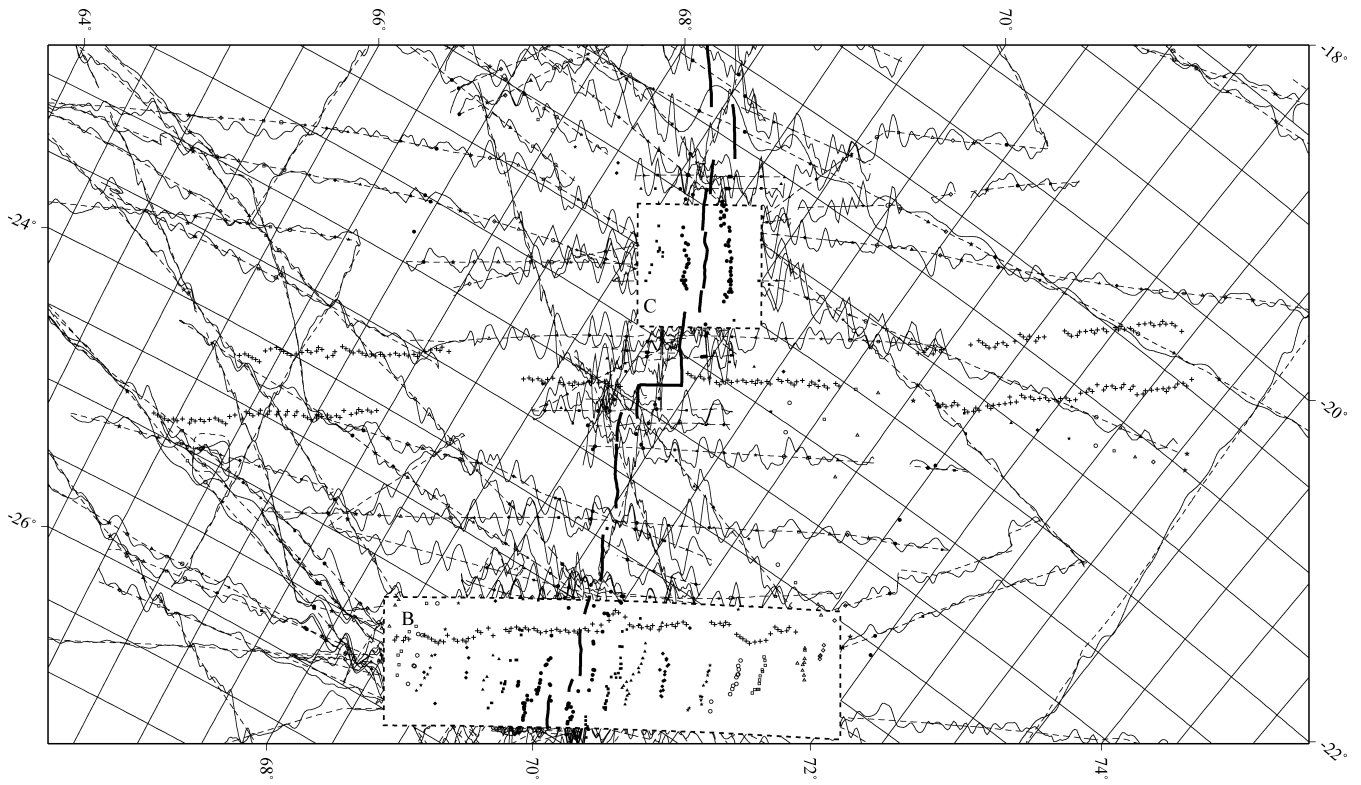
Figure A2–A6. (*Continued.*)
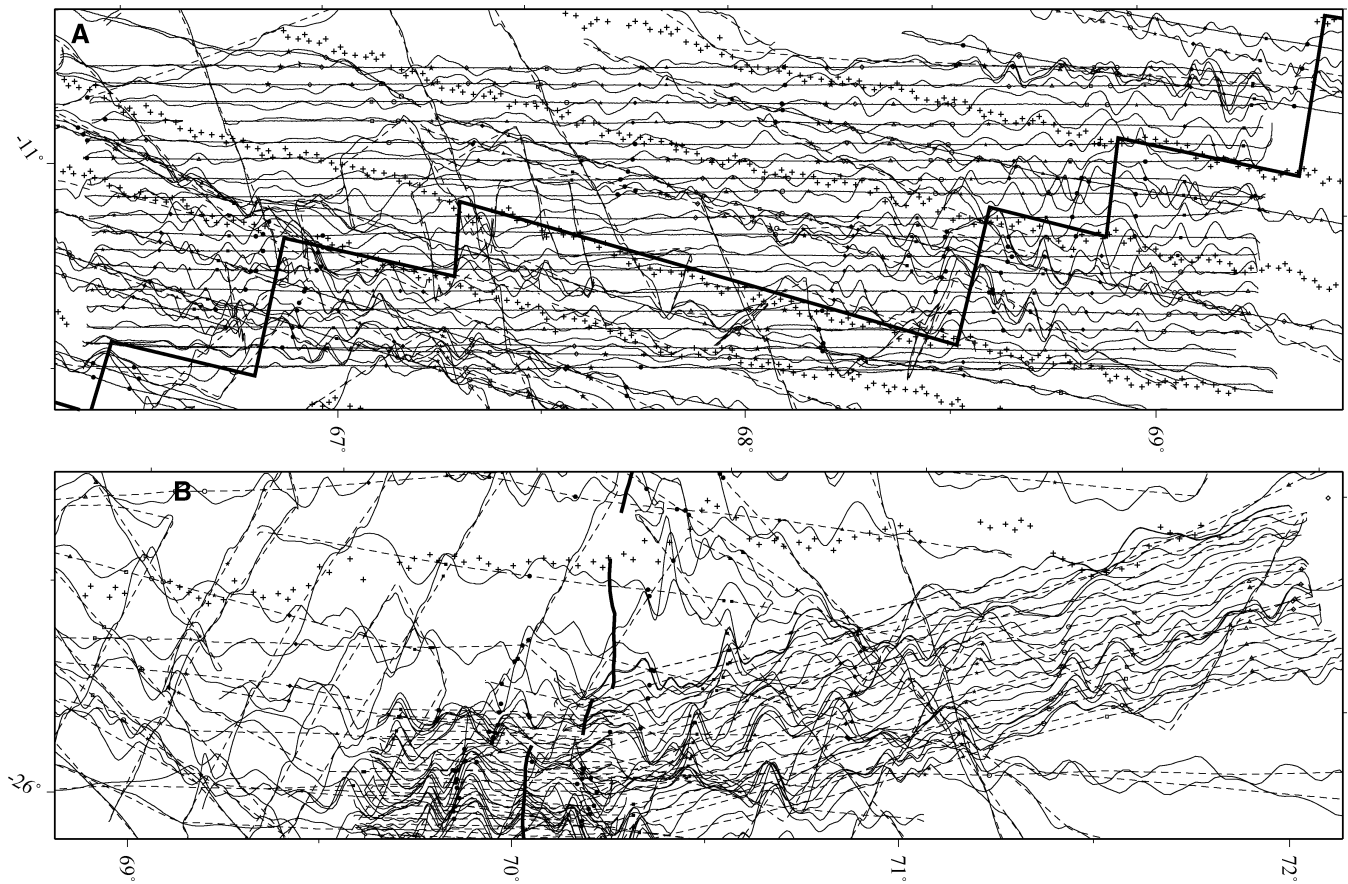
Figure A2–A6. (*Continued*.)

Figure A7: panel (a) shows magnetic profiles from area A of Fig. A3. Panel (b) shows magnetic profiles from area B of Fig. A6.